frontiers | Frontiers in Earth Science

TYPE Original Research
PUBLISHED 07 March 2024
DOI 10.3389/feart.2024.1354317

OPEN ACCESS

EDITED BY
Stanislaw Mazur,
Polish Academy of Sciences, Poland

REVIEWED BY
Jean-louis Vigneresse,
Université de Lorraine, France
Shengyao Yu,
Ocean University of China, China

*CORRESPONDENCE
Wenjiao Xiao,
wj-xiao@mail.iggcas.ac.cn
Miao Sang,
sangmiao@ms.xjb.ac.cn

RECEIVED 12 December 2023
ACCEPTED 13 February 2024
PUBLISHED 07 March 2024

CITATION
Huang P, Yan Z, Xiao W, Sang M, Mao Q and Abuduxun N (2024), Early cretaceous multi-stage extension in the North Dabie complex in the eastern central China: insights from structural and geochronological data. *Front. Earth Sci.* 12:1354317. doi: 10.3389/feart.2024.1354317

Early cretaceous multi-stage extension in the North Dabie complex in the eastern central China: insights from structural and geochronological data

Peng Huang[1,2,3], Zhen Yan[4], Wenjiao Xiao[1,2,3]*, Miao Sang[1,2,3]*, Qigui Mao[1,2,3] and Nijiati Abuduxun[5]

[1]National Key Laboratory of Ecological Safety and Sustainable Development in Arid Lands, Xinjiang Institute of Ecology and Geography, Chinese Academy of Sciences, Urumqi, China, [2]Xinjiang Key Laboratory of Mineral Resources and Digital Geology, Urumqi, China, [3]College of Earth and Planetary Sciences, University of Chinese Academy of Sciences, Beijing, China, [4]Institute of Geology, Chinese Academy of Geological Sciences, Beijing, China, [5]Xinjiang Key Laboratory for Geodynamic Processes and Metallogenic Prognosis of the Central Asian Orogenic Belt, School of Geology and Mining Engineering, Xinjiang University, Urumqi, China

A dominantly NW-SE directed extensional tectonics in the Early Cretaceous significantly reworked the Late Permian-Triassic orogenic framework of the Dabie orogenic belt. The North Dabie complex (NDC) is the principal domain recording this tectonic event. However, the precise structure-kinematic architectures, particularly those observed in the ductile regime, along with the respective time scales for different extensional stages, have not been adequately established. This significantly impedes our comprehensive understanding of the extensional style and deformation history in the North Dabie complex. To better address these issues, we conducted a systematic structural study and LA-ICP-MS zircon U-Pb dating of the pre-, syn-, and post-kinematic intrusions and syn-kinematically metamorphosed high-grade gneisses/migmatites of the NDC. Our results demonstrate that the extensional deformation in the NDC may initiate at ca. 144 Ma, which is characterized by a pervasive NW-SE oriented coaxial plastic flow in the ductile regime of the middle-lower crust. A large-scale detachment processing zone subsequently started activating at ca. 140 Ma at the upper-middle level of the middle crust, and concentratedly accommodated the extensional strain by top-to-NW ductile shearing. Locally, there was uprising of sub-magmatic flow in the atatexite-diatexite from the deeper lower crust taking place in the manner of top-to-outward shearing as early as ca. 137 Ma. This composite process of extension manifests vertical strain partitioning across the ductile middle-lower crusts and progressive strain localization during the lithospheric thinning. The NW-SE orientation dominated extensional tectonics was strongly driven by the westward subduction of the Paleo-Pacific oceanic plate during the Late Mesozoic.

KEYWORDS

extensional tectonics, Early Cretaceous, multi-stage extension, multi-style crustal, North Dabie complex

Keypoints

- The North Dabie extensional complex formed under NW-SE oriented extensional/transtensional strain regime in the Early Cretaceous
- Ca. 144–138 Ma NW-SE oriented coaxial dominated plastic flow penetrated the middle-lower crust of the Dabie lithosphere
- 140–130 Ma large-scale low-angle detachment processing zone localized the extensional strain by top-to-NW ductile shearing in the middle crust
- Sub-magmatic flow actively ascended from the lower crust in the diapiric manner during ca. 137–125 Ma

1 Introduction

The Dabie orogenic belt (DOB), as the eastern extension of the ~2000 km long Qinling orogen, was formed by the continental collision and subsequent northward subduction of the South China Block (SCB) beneath the North China Block (NCB) more than ~120 km deep in the Triassic (Zhang et al., 1996; Ye et al., 2000; Zhang et al., 2013a; Zheng et al., 2013; Dong and Santosh, 2016; Dong et al., 2022). The continental deep subduction gave birth to one of the most spectacular formations of the high pressure-ultrahigh pressure (HP-UHP) metamorphic rocks on our planet (Wang et al., 1989; Xu et al., 1992; Okay et al., 1993; Hacker et al., 1995; Li et al., 2000; Li et al., 2007; Zheng, 2008; He et al., 2022). The HP-UHP orogenic belt of the DOB was significantly reworked by extensional tectonics in the Early Cretaceous. (Faure and Lin, 1998; Ratschbacher et al., 2000; Wu et al., 2007a; Wang et al., 2007; Wang et al., 2011; Deng et al., 2014; Zhang et al., 2014; Lin et al., 2015; Wang et al., 2018; Yang et al., 2020).

Previous studies have already revealed that the North Dabie complex (NDC) is showcased as the primary domain on which the Early Cretaceous structures overprinted in the DOB (Ratschbacher et al., 2000; Li et al., 2002; Faure et al., 2003; Wang et al., 2007; Wang et al., 2011; Lin et al., 2015). It is widely agreed that large-scale detachment(s) and the development of gneissic/migmatitic domes occurred progressively in the NDC. Several kinematic-structural models have been proposed to interpret the extensional processes, such as the lateral extrusion model (Wang et al., 1998), isostatic rolling hinge model (Ratschbacher et al., 2000), detachment flow model (Wang et al., 2011), double-directed or down-to-the-outward collapse models (Zhong et al., 1998; Suo et al., 2001; Hou et al., 2012), and evolving detachment in a Metamorphic Core Complex (MCC) (Lin et al., 2015; Ji et al., 2017). These models have greatly enhanced our understanding of the complex extensional evolution of the North Dabie.

The above-mentioned models commonly demonstrate that development of a detachment is a critical mechanism for the extensional deformation. However, reconstructing the detachment has encountered substantial challenges; since the initial occurrence of the detachment has been greatly modified and separated into different segments due to the extension induced uplift and accompanied tectonic denudation. Timing constraint on the potential segments is considered one of critical approaches to reconstruct the detachment, but further complications have been faced in the case of the NDC. This is mainly because intermittent reheating of magmatism in the region disturbed or even reset the Ar^{40}/Ar^{39} isotopic systems, which are traditionally used to constrain the timing of deformation for the mylonitic shear zones (Hou et al., 2007; Ji et al., 2017; Ratschbacher et al., 2000; Wang et al., 2011). In addition, less attention has been paid to the structural variations and kinematic differentiations of the ductilely stretching middle-lower crust as a whole in the NDC, particularly those beneath the detachment. Structural variations and kinematic differentiations across the ductile regime of the crust are crucial indicators for the flow dynamics as the strain selectively partitions within the rheologically heterogeneous continuum during lithospheric-scale thinning (Wiest et al., 2019).

The close spatial and temporal association of magmatite, anatexite, and metamorphic fluids with crustal-scale shear zone systems has been extensively observed in numerous geological settings (Vanderhaeghe, 2001; Albertz, 2006; Ávila et al., 2019; Zhang et al., 2023). Evolution of the melts/fluids and processing of the deformation structures are regarded as manifestation of self-organization for the highly non-equilibrium orogenic systems to efficiently reduce the energetic gradients (Brown and Solar, 1998). Zircon crystallized or overgrown from the melts in the syn-kinematic intrusions and anetexites, or precipitated from the metamorphic fluid in syn-kinematically metamorphosed tectonites provides valuable constraints on the temporal scale of the high-grade deforming complex (Hanmer et al., 1997; Brown and Solar, 1998; Nzenti et al., 2006; Boffadossi et al., 2020; Jolivet et al., 2021).

In this study, we conducted a comprehensive analysis of the structural and micro-tectonic characteristics of the bounding mylonitic shear zones confining the North Dabie complex and the deformed-metamorphosed interior domains within the complex. Additionally, we conducted zircon LA-ICP-MS U-Pb dating on several crucial samples, including pre-, syn-, and post-kinematic igneous intrusions, as well as syn-kinematically metamorphosed gneisses/migmatites. Combining our newly obtained data with previous published results, we reconstruct a thick, large-scale detachment processing zone and a kinematic-structural model for the North Dabie extensional tectonics. Finally, with these findings, we attempt to reconstruct the tectono-structural evolution of this extensional event in the NDC.

2 Geological setting

The DOB is composed of several litho-tectonic domains from north to south including the Beihuaiyang belt, Dabie metamorphic complex belt (DMCB), and Yangtze foreland fault-and-thrust belt, respectively (Figure 1). The DMCB could be further divided into the autochthonous orogenic basement known as the North Dabie complex (NDC) and an overlying stacking-suit of exhumed structural slices. These structural slices include from bottom to top the para-autochthonous South Dabie complex (SDC), allochthonous gneissic slice known as the Central Dabie HP/UHP complex (CDHC) with its western counterpart known as Xinxian-Hong'an HP/UHP complex, and HP schistose slice referred to as the Susong Group (Faure and Lin, 1998; Faure et al., 1999; Faure et al., 2003). These different litho-tectonic domains documented a sequence of tectonic events throughout the DOB's

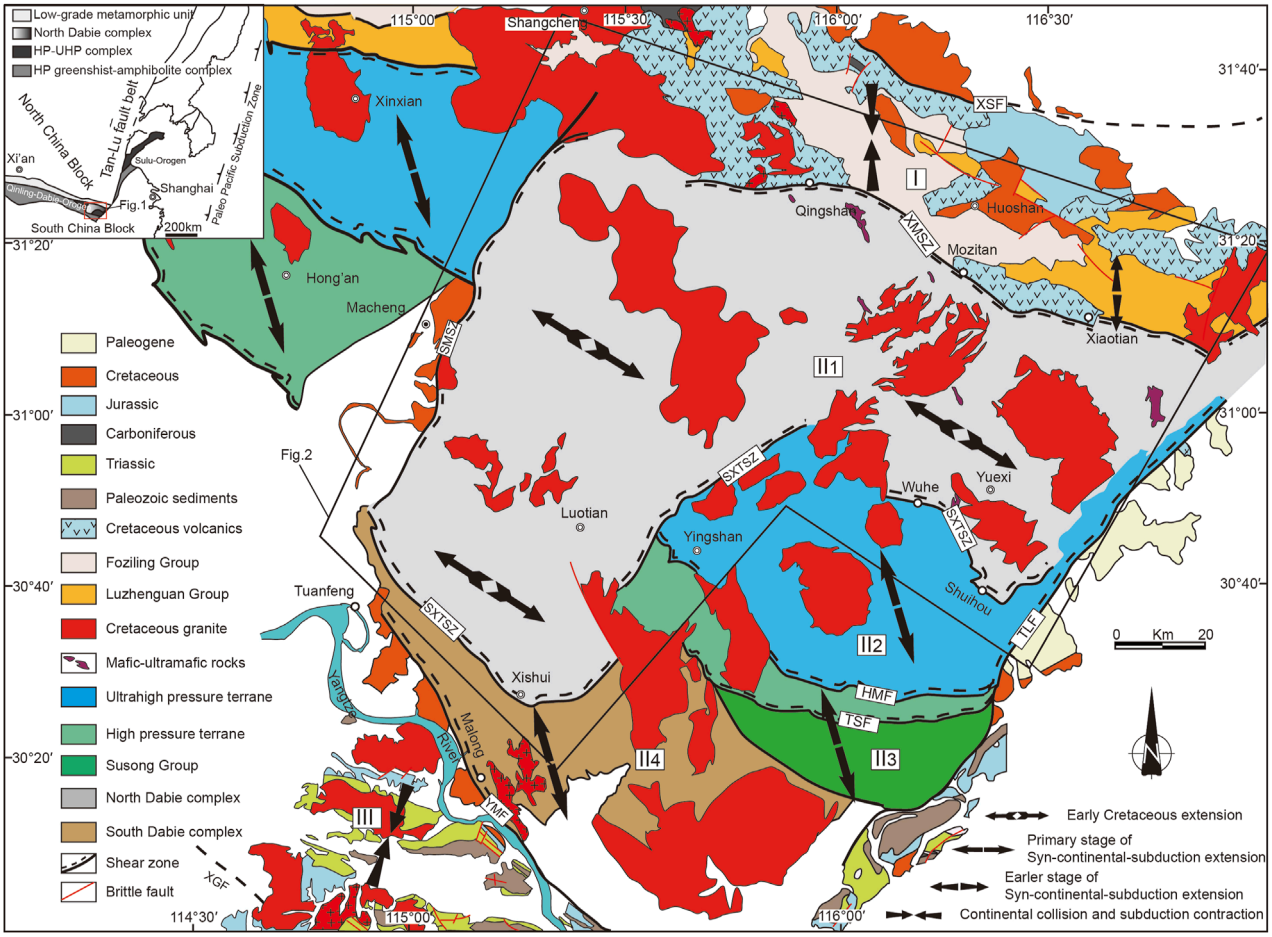

FIGURE 1
Geological map showing main tectonic domains of the Dabie orogen (modified after Xu et al., 2007). I = Beihuaiyang belt; II = Dabie metamorphic complex belt; II1 = North Dabie complex; II2 = Central Dabie HP-UHP complex; II3 = Susong Group; II4 = South Dabie complex; III = Yangtze foreland fold-and-thrust belt; XMSZ = Xiaotian-Mozitan shear zone; SMSZ = Shangcheng-Macheng shear zone; SXTSZ = Shuihou-Xishui-Tuanfeng shear zone; TLF = Tan-Lu Fault; HMF = Hualiangting-Mituo Fault; TSF = Taihu-Shanlong Fault; YMF = Yindian-Malong Fault.

evolution (Table 1). Information regarding continental collision is predominantly retained in the Beihuaiyang belt and the Yangtze foreland fold-and-thrust belt. The dominant amphibolite-facies rocks of the CDHC are retrograded from eclogite-facies HP-UHP rocks; they exhibits records of the primary exhumation phase that translated the HP/UHP rocks from mantle depths to middle-lower crustal levels. The locally contained elcogite blocks in the CDHC preserve information of the high-pressure to ultra-high-pressure metamorphic processes. The Early Cretaceous extensional deformation was mainly displayed in the NDC, which is also responsible for the final exhumation of the HP/UHP rocks from middle-lower crust to the Earth surface.

The Beihuaiyang belt mainly consists of Paleozoic turbiditic rocks of the Foziling Group and Neoproterozoic orthogneiss and amphibolite complex of the Luzhenguan Group. The rocks in this belt underwent strong deformation and greenschist facies to amphibolite facies metamorphism. They unconformably underlie the Jurassic sedimentary strata (Chen et al., 2003; Zheng et al., 2005; Huang et al., 2016). Deformation structures manifest N-NNE dipping foliation and isoclinal folds with axial planes parallel to the foliation, along with near N-S directed stretching lineation and top-to-south thrusting (Faure et al., 2003; Lin et al., 2005), indicating N-S oriented compression and northward subduction. Geothermobarometer demonstrated a geothermal gradient of 10°C/km for the deformation (Wang et al., 2012). $^{40}Ar/^{39}Ar$ dating of muscovite and U-Pb dating of rutile and titanite suggested 271–260 Ma for the deformation. This deformation is interpreted as continental collision between the NCB and the SCB (Faure et al., 2003; Ratschbacher et al., 2006; Liu et al., 2013; Zhao et al., 2023). Augen gneisses of the Luzhengguan Group near the Xiaotian-Mozitan shear zone also documented a later near N-S oriented extensional deformation, characterized by northward dipping foliation and top-to-north collapse, which was interpreted as a syn-continental-subduction extension responsible for early stage of exhumation for the subducted rock slices (Lin et al., 2005). The deformation took place during 250–235 Ma (Hacker et al., 1995; Zheng et al., 2007) in a relatively higher geothermal gradient of 10°C–20°C/km (Zhao et al., 2023).

10.3389/feart.2024.1354317

TABLE 1 Tectonic domains and tectonic events of the Dabie orogenic belt.

Tectonic domain	Tectonic event	Deformation regime	Deformation	Geothermal gradient	Time scale	References
Beihuaiyang	Continental collision	N-S oriented contraction	N-S oriented stretching lineaiton and top-to-south shearing, southward thrusting	10°C/km	270–252 Ma	Faure et al., 2003; Liu et al., 2013; Ratschbacher et al., 2006; Zhao et al., 2023
	Early stage syn-subduction exhumation	N-S oriented extension	N-S oriented stretching lineaiton and isoclinal folding, top-to-north shearing, northward collapse	10–20°C/km	250–235 Ma	Lin et al., 2015; Faure et al., 2003
Yantze foreland	Continental collision	N-S/NNW-SSE oriented contraction	E–W to NE–SW trending upright or southward overturned folding, southward thrusting	20–30°C/km	245–205 Ma	Faure et al., 2003; Li et al., 2010
Central Dabie/Xinxian-Hong'An	Continental deep subduction and HP-UHP metamorphism	N-S oriented contraction	N-S oriented stretching lineation, Top-to-south shearing, southward thrusting	5°C/km	244–230 Ma	Li et al., 2000; Xu et al., 2007; Zheng et al., 2008; Lin et al., 2009
Central Dabie/Hong'An and South Dabie	Primary stage syn-subduction exhumation of the HP/UHP rocks and amphibolite facies retrogression	NNW-SSE oriented extension	NNW-SSE oriented stretching lineaiton and top-to-NNW shearing	10–20°C/km	230–205 Ma	Zheng et al., 2007; Li et al., 2013; Lin et al., 2015; Faure et al., 1999; Hacker et al., 2000
North Dabie	Final stage exhumation of the HP/UHP rocks, regional extension and delamination of the orogenic root	NW-SE oriented extension	NW-SE oriented stretching lineation and top-to-NW shearing	>30°C/km	Early Cretaceous	Ratschbacher et al., 2000; Hacker et al., 2000; Wang et al., 2011; Zhang et al., 2014; Chen et al., 2006; Lin et al., 2015

The Yangtze foreland fold-and-thrust belt consists of the Proterozoic metamorphic rocks and unconformably overlying Neoproterozoic to Triassic sediments, which underlie the undeformed cover of Jurassic sedimentary strata (Schmid et al., 1999). Deformation structures are characterized by a sequence of south vergent imbrication of E-W/NE-SW trending tight and overturned or recumbent fold nappes separated by southward thrusts (Li et al., 2010; Faure et al., 2003). These thrusts merged deeply onto a greater north dipping decollement reflected by the seismic profile, which was interpreted as the remnant of north-directed structures resulting from the subduction of the Yangtze terrane under the Dabie terrane (Dong et al., 2004). This fold-and-thrust structural association demonstrates a NNW-SSE directed regional shortening mainly due to continental amalgamation between the Yangtze terrane and the Dabie terrane. $^{40}Ar/^{39}Ar$ dating of muscovite provided a time span of ca.245–205 Ma for the deformation (Li et al., 2010, and reference therein).

In the para-autothonous to allochthonous stacking suit, the lowermost stacked rock slice–SDC–mostly consists of granitic gneisses, biotite-amphibolite-plagioclase gneisses, and minor amphibolite. Rocks in this domain are metamorphosed under amphibolite facies conditions (Hacker et al., 1995; Hacker et al., 2000). The SDC was designated as a slice of para-autochthonous basement of the Yangtze Craton due to its absence of UHP rocks (Faure et al., 2003). The allochthonous structural slices of the CDHC mainly consists of amphibolite facies orthogneiss and paragneiss containing abundant HP/UHP eclogite blocks, and minor phengite schist, marble, and quartzite. The Susong Group is dominated by micaschists, quartzites and metabasites, which underwent blueschist–green schist facies metamorphism (Zheng, 2008; Shi et al., 2014). Structural geometry in these structural slices exhibits a consistent SSE-to SSW-dipping monoclinic foliation and NW-SE to NNW-SSE-plunging stretching lineation, with top-to-NW/NNW kinematic indicators (Hacker et al., 1995; Wang et al., 1998; Hacker et al., 2000; Faure et al., 2003). These deformation structures were regarded as evidence of a syn-continental-subduction extension that accounted for the primary stage of exhumation of the HP/UHP slices from mantle depths to middle-

lower crustal levels (Okay et al., 1993; Maruyama et al., 1994; Faure et al., 2003; Lin et al., 2009). P-T paths and geochronological data suggest a geothermal gradient of ca. 10°C–20°C/km and a time range of 230–205 Ma for the deformation (Ames et al., 1996; Ayers et al., 2002; Zheng et al., 2007; Zheng, 2008).

Mineral inclusions of micro-diamond, coesite in the eclogite blocks within the paragneisses of the CDHC indicate that UHP metamorphic conditions are 700°C–850°C and 2.8–4 Gpa at a geothermal gradient as low as 5 °C/km (Wang et al., 1995; Carswell et al., 2000; Liou et al., 2000). Garnet and omphacite form N-S directed lineation and S-dipping foliation; asymmetric garnet porphyroclasts indicate top-to-south kinematics (Xu et al., 2002). These structures were interpreted as deformation of continental deep subduction (Hacker et al., 1995; Li et al., 2010). SHRIMP zircon U-Pb dating of coesite-bearing domains demonstrates that the timing of the UHP metamorphism is ca. 242–227 Ma (Xu et al., 1992; Yang et al., 2003; Liu et al., 2004; Wan et al., 2005; Liu et al., 2008).

The NDC is characterized by the Early Cretaceous extensional deformation. It is bounded by the Xiaotian-Mozitan shear zone (XMSZ) to the north, Shuihou-Xishui-Tuanfeng shear zone (SXTSZ) to the south, Shangcheng-Macheng shear zone (SMSZ) to the west, and Tan-Lu fault to the east (Figure 1). It is dominated by foliated dioritic, tonalitic, and granitic orthogneisses and layered migmatites (Bryant, 2004; Zhao et al., 2005; Xie et al., 2010). Structural studies demonstrate that the NDC is characterized by an asymmetrically dome-shaped metamorphic culmination and NW-SE directed stretching lineation. Top-to-NW shearing dominated the deformation. The extensional deformation took place in the Early Cretaceous with a deformation peak at ca. 130–120 Ma and a higher geothermal gradient above 30 °C/km (Faure et al., 1999; Hacker et al., 2000; Xu et al., 2002; Chen et al., 2006; Liu et al., 2011; Zhang et al., 2014).

Early Cretaceous granitoids are extensively distributed in the DOB, with a significant concentration in the eastern part of the DMCB, accounting for almost half of the exposed surface area (Ratschbacher et al., 2000). They primarily consist of 143–117 Ma granites, granodiorites, and diorites (Xu et al., 2002; Wang et al., 2007; Deng et al., 2014). The 143–130 Ma granitoids exhibit adakitic characteristics with high Sr contents and elevated La/Y and Sr/Y ratios, which probably originated from partial melting of the thickened eclogitic lower crust or magma mixing between melts from delaminated lower crust and mantle-derived magma (Wang et al., 2007; Zhang et al., 2013b). In contrast, the <130 Ma granitoids with normal geochemical affinity of granites were interpreted to be formed by partial melting of plagioclase-bearing granulite from a thinned crust (Wang et al., 2007; He et al., 2011). Both types of granitoids contain abundant inherited zircon relicts from the Neoproterozoic. Additionally, there are mafic-ultramafic dykes and gabbro intrusions present as secondary occurrences of the Cretaceous magmatism (Xu et al., 2012; Zhang et al., 2015; Li et al., 2021). The onset of mafic-ultramafic igneous activity occurred at ca. 130 Ma slightly later than the commencement of intermediate-acid magmatism (Xu et al., 2012; Zhang et al., 2015). These mafic-ultramafic rocks are considered to be derived from an enriched mantle source that has been contaminated by the foundered lower eclogitic crust, as indicated by major and trace element compositions as well as isotopic characteristics (Xu et al., 2012; Zhang et al., 2015).

3 Structural and deformation features

3.1 The bounding mylonitic shear zones

Three mylonitic bounding shear zones, which named as the Xiaotian-Mozitan shear zone (XMSZ), Shangcheng-Macheng shear zone (SMSZ), and Shuihou-Xishui-Tuanfeng shear zone (SXTSZ) (Figure 2), separate the NDC from the Beihuaiyang belt to the north, the exhumed rock slice of Xinxian-Hong'an UHP/HP complex to the west, the SDC to the south, and the CDHC to the east, respectively.

They are marked by 0.5–1.5 km thick high-strain zones of granitic, biotite-granitic or granodioritic proto-mylonite to ultra-mylonite sequences (Figures 3A–C). The mineral assemblages of chlorite + epidote + biotite + muscovite and amphibolite + biotite + plagioclase are commonly observed, indicating green schist facies to amphibolite facies conditions for the deformation. Mineral shape fabrics in the zones are dominated by typical S-L tectonites. Fine-grained matrix of highly recrystallized quartz, mica, and some feldspar forms clear cleavage domains; and strongly stretched quartz grains and their aggregates, alignment of porphyroclasts (e.g., feldspar, amphiboles) form pronounced stretching/mineral lineations (Figures 4A,B; Figures 5A,B; Figures 6A,B). Most quartz grains were dynamically recrystallized by sub-grain rotation (SGR) and/or high-temperature grain boundary migration (GBM), accompanied by variable amounts of bulging (BLG) recrystallization of feldspar and various crystalline cracks or fractures on amphiboles (Figures 4A,B; Figures 5A,B; Figures 6A,B). These fabrics indicate a thermal condition of 450°C–530°C (Passchier and Trouw, 2005), corresponding to upper greenschist facies to lower amphibolite facies for the deformation (Bucher, 2023). In addition, our field and microscope observation results demonstrate that a consistent fabric gradient traverses the mylonite zones toward the interior of the NDC, which is characterized by a growing degree of compositional segregation, gradually amplified grain sizes and increasingly distinctive lobateness in dynamically recrystallized quartz grains. In particular, recrystallization type of the quartz shifts from predominantly SGR to a combination of SGR and GBM, and ultimately to independent GBM. This trend demonstrates that the deformation temperature is gradual increasing, whereas associated flow stress simultaneously decreases.

In general, there is a notable consistency in both geometry and kinematic/strain-orientation among these zones. The strikes of the shear zones exhibit curvature in different portions. The XMSZ has a gentle north-ward bulging at its middle part, and the SXTSZ shows an S-shaped strike. Even the seemingly straight-striking SMSZ deflects NE-ward at its northern end. Although periodic occurrences of patchy granitic intrusions interrupt the shear zones, these curves indicate a potential for continuity between these framing shear zones surrounding the NDC. Mylonitic foliations generally show outward dipping (with reference to the metamorphic NDC as the inside core) with a wide range of dipping angles. The lineations in the mylonite exhibit a remarkable concentration of plunging directions in the fields of 300/120 ± 20° (azimuth notation), featuring plunging angles ranging from sub-horizontal to sub-vertical and pitches varying from strike-slip type to down-dip type (Figures 2A–C). Asymmetric intrafolial folds, σ- or δ-type porphyroclasts, S-C fabrics, and shear

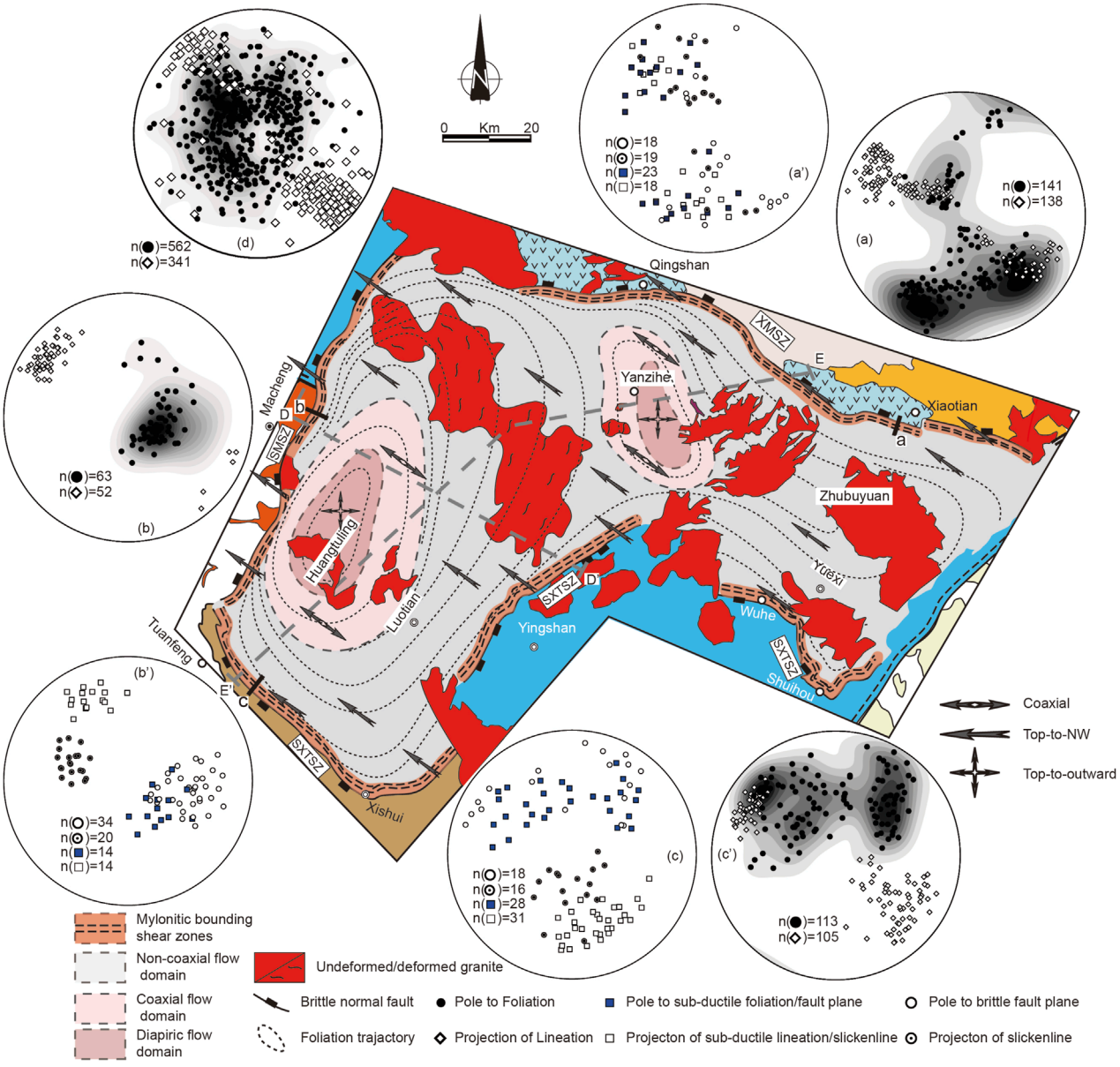

FIGURE 2
Structural and kinematic data of the North Dabie metamorphic complex. **(A–C)** Projection for ductile fabrics of the bounding shear zones of the XMSZ, SMSZ, and SXTSZ respectively **(A'–C')** Projection for sub-ductile and brittle fabrics of the bounding shear zones; **(D)** Projection for ductile fabrics of the gneiss and migmatite in the interior of the North Dabie. All projections are plotted at equal area and in lower hemisphere.

band boudinages (Figures 4A–C; Figures 5A–C; Figures 6A–D) universally indicate top-to-the-NW/NWW kinematics. These observations yield apparent sinistral shearing for the XMSZ (Figure 4C) and dextral shearing for the NW-SE striking segment of the WXTSZ (Figure 6C) in map view, and normal slipping for the SMSZ (Figure 5C) and reverse slipping for the NNE-SSW striking segment in cross-sections (Figure 6D).

The bounding mylonitic shear zones were overprinted by sub-ductile shearing and brittle faulting sequentially (Figures 2A–C). The sub-ductile shearing was processed heterogeneously in centimeter-to-meter thick small shear zones that run parallel to or cut at small angles with the dominant foliations, resulting in either parallel (Figure 4D; Figure 5D) or anastomosing distribution patterns. Chloritization of amphiboles and sericitization of plagioclase prophyroclasts are common retrograde expressions in this small shear zones, leading to darkening of the small shear zones at outcrops (Figure 4D). Lineations/striations on the sub-ductile slipping surfaces are dominated by oblique type (Figures 2A'–C'), corresponding to a universal down-ward motion (Figure 4D; Figure 5D) and concurrent lateral displacements along the strikes (Figures 2A–C). Sharply dipping brittle normal faults cut both the ductile mylonite (Figure 5C; Figure 5E) and sub-ductile shear zones. The major breccia zones are generally located at the outer edge of the ductile mylonitic zones, along which Xiaotian and Macheng

10.3389/feart.2024.1354317

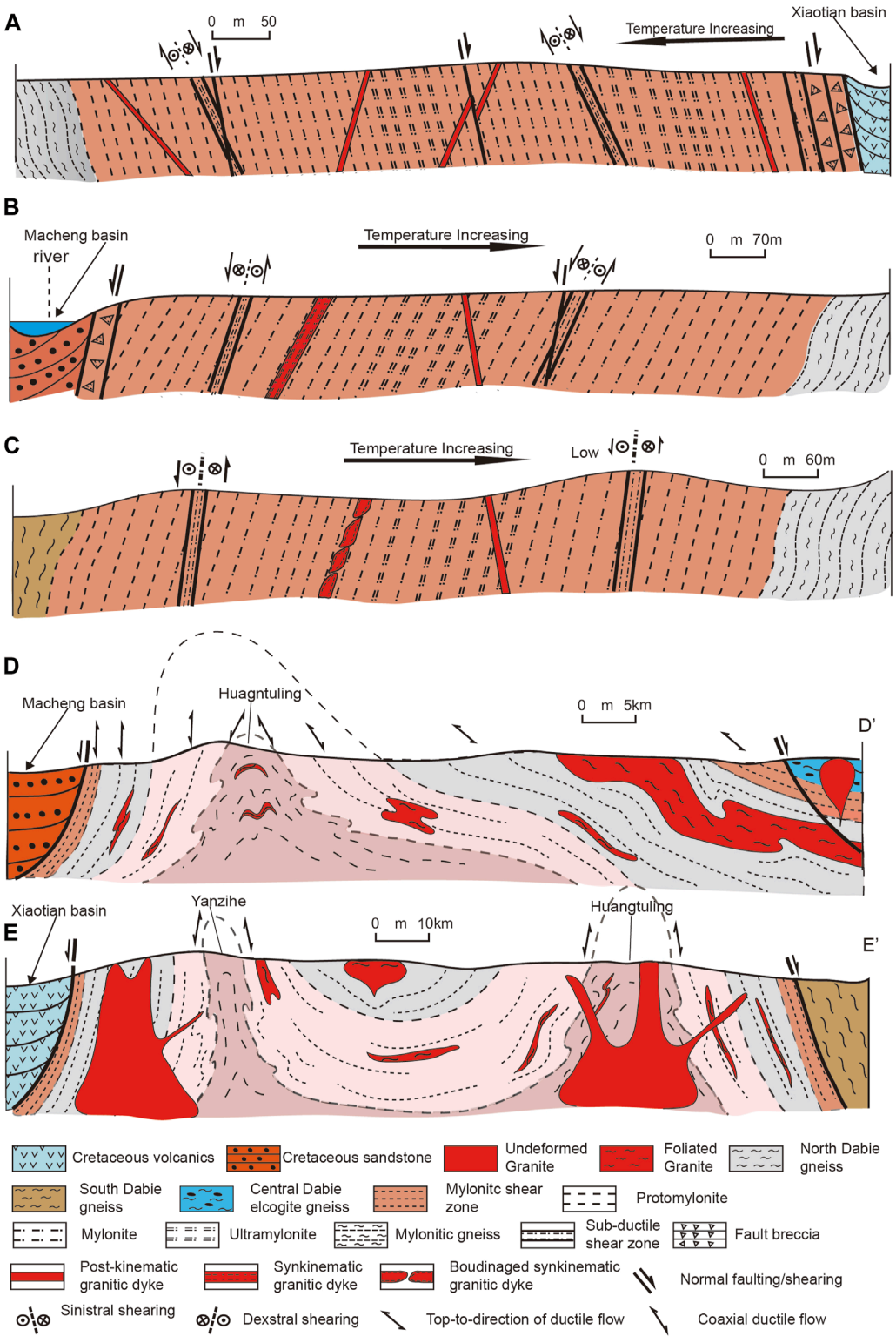

FIGURE 3
(A–C) Cross-sections showing tectonites, subductile shearing and brittle faulting overprinting across the bounding mylonitic shear zones, locations are marked in Figure 2. **(D-D′ and E-E′)** Overall cross-sections of the North Dabie metamorphic complex parallel and perpendicular/sub-perpendicular to the mountain range trending, respectively.

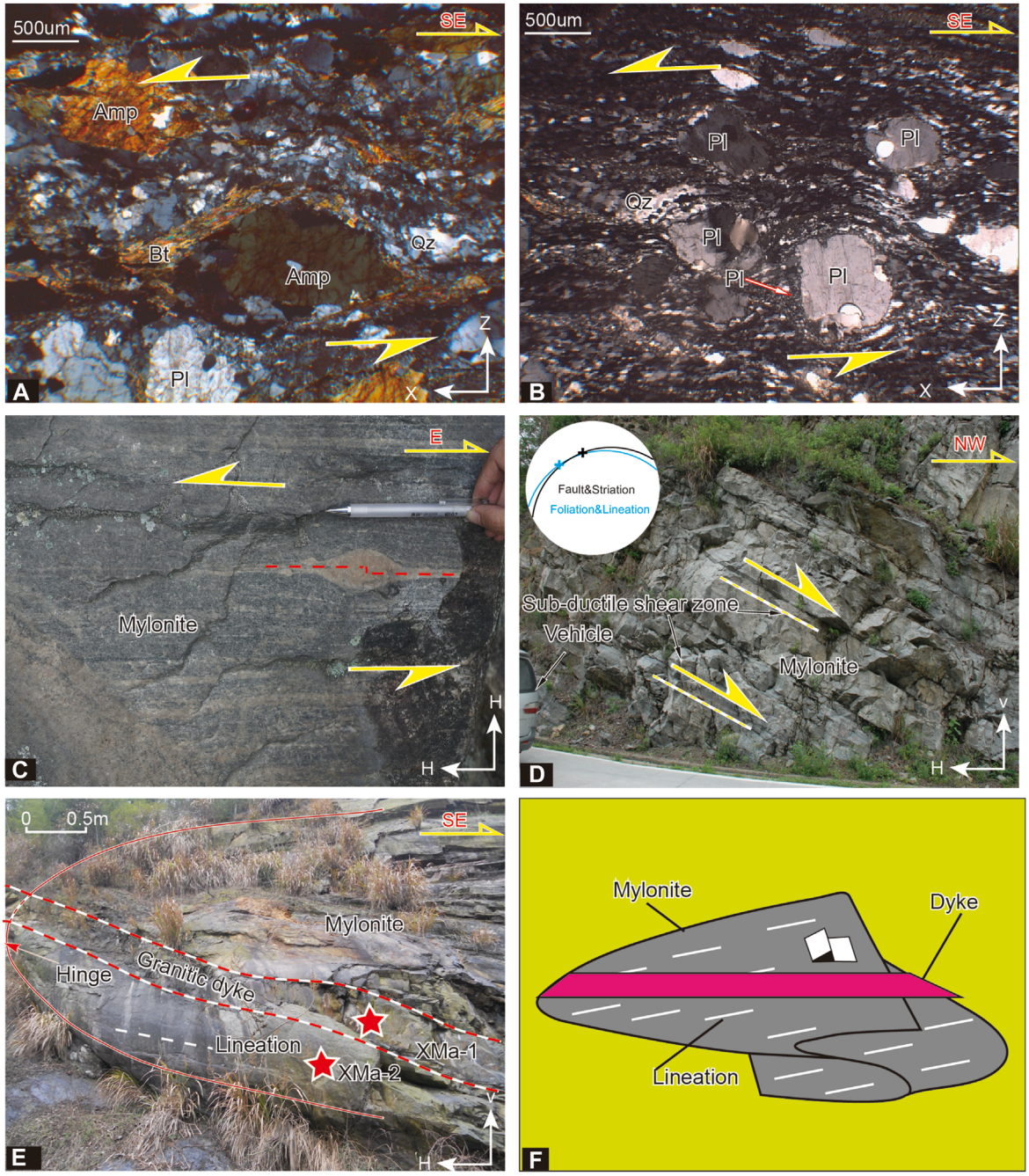

FIGURE 4
Structural features of the XMSZ. **(A)** σ-type amphibole porphyroclasts of dioritic mylonite with intra-crystalline cracks and asymmetric strain shadow formed by biotite on the lee sides, indicating a top-to-the-NW shearing. **(B)** Core-mantle fabrics of granitic mylonite consisting of felspathic porphyroclasts and fine orphyroclasts of BLG recrystallization. Stair stepping of the tails indicates a top-to-the-NW shearing. **(C)** σ-type mega-K-feldspar showing left-lateral stair stepping. **(D)** Mylonite of the major shear zone and retrograde minor smaller sub-ductile normal shear zones (dark in color) parallel to the mylonitic foliation overprinted on the mylonite. **(E)** A big sheath fold cut by a granitic dyke. **(F)** Schematic drawing of the sheath fold and the later injection of the dyke. Abbreviation: Bt = biotite; Amp = amphibolite; Pl = plagioclase; Qz = quartz. Photomicrographs are taken under cross polarized light. X and Z represent directions of the longest and shortest principal strain axes, respectively; H and V represent horizontal and vertical directions, respectively.

volcano-siliciclastic basins were developed in the north and west respectively (Figure 3).

In addition to voluminous plutons forming sharp intrusive contact with the mylonite (Figure 5E), multiple dykes in the mylonitic shear zones show various occurrences. Some dykes with straight boundaries intersect the country mylonites at high angles with the foliation and their interior portion does not exhibit ductile deformation (Figures 4E,F). Some

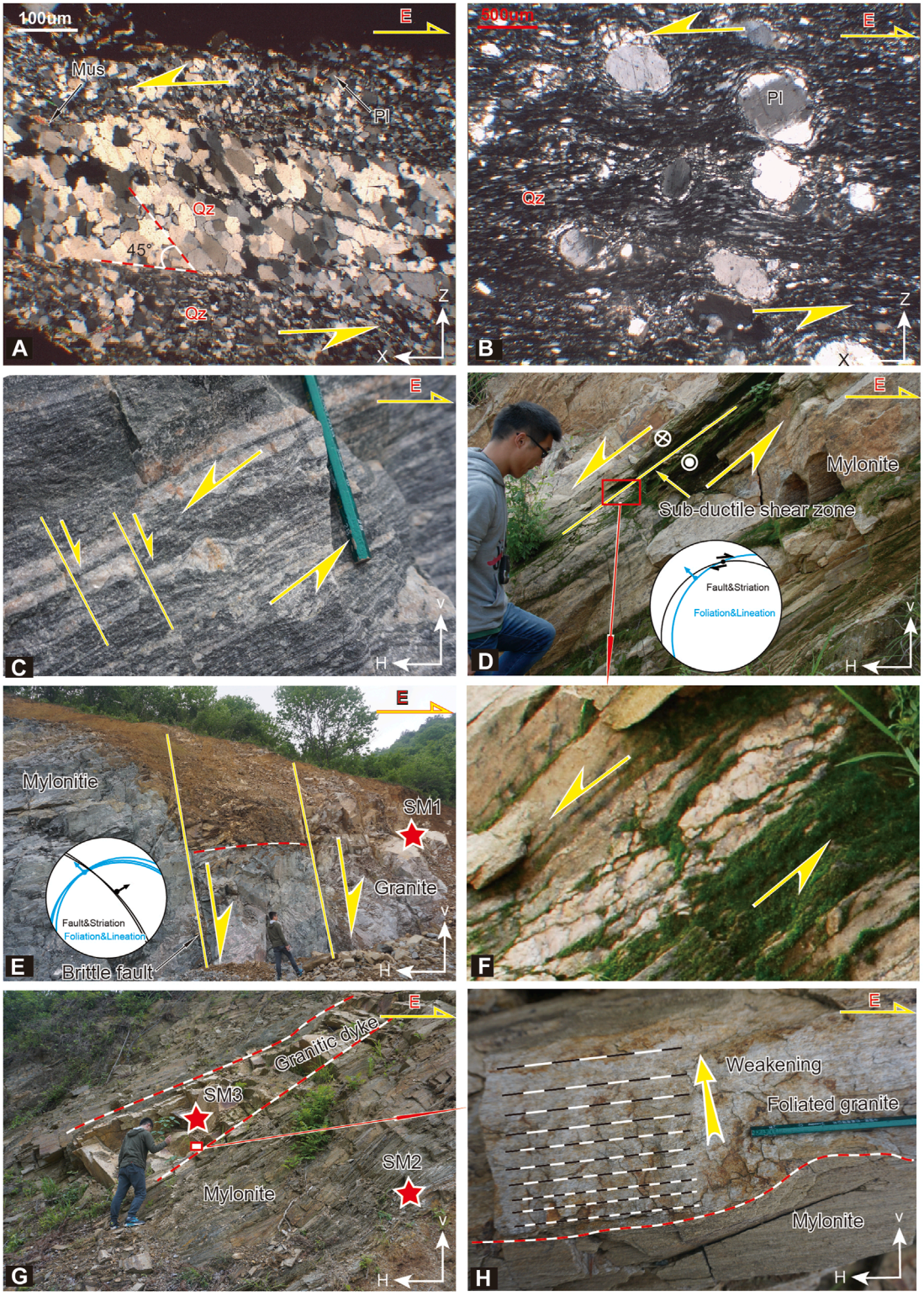

FIGURE 5
Structural features of the SMSZ. **(A)** Oblique foliation defined by elongate quartz grains derived from SGR recrystallization, indicating a top-to-NW shearing. The oblique foliation makes an angle of ca. 45° to the C-plane, indicating a simple shearing dominated deformation. **(B)** Felspathic porphyroclasts surrounded by recrystallized feldspar by BLG to form core-mantle fabrics, and asymmetric tails indicating a top-to-NW shearing. **(C)** σ-type K-feldspar megacryst in the northern segment of the shear zone, indicating a top-to-NW shearing. **(D)** Sub-ductile normal-sinistral shear zone overprinting on the ductile shear zone. **(E)** Granitic mylonite of the SMSZ, with sharply dipped brittle normal faults crosscutting both the mylonite and a granitic pluton that intruded into the mylonite. **(F)** Oblique alignment of sub-ductile breccia forming an S-C pattern indicating normal shearing. **(G)** A syn-kinematic granitic dyke in the mylonite zone. **(H)** Foliation of the dyke shows weakening from the edge to the center. Photomicrographs are taken under cross polarized light. Abbreviation of the minerals and arrows on the corners of the photos keep the same connotations with those in Figure 4.

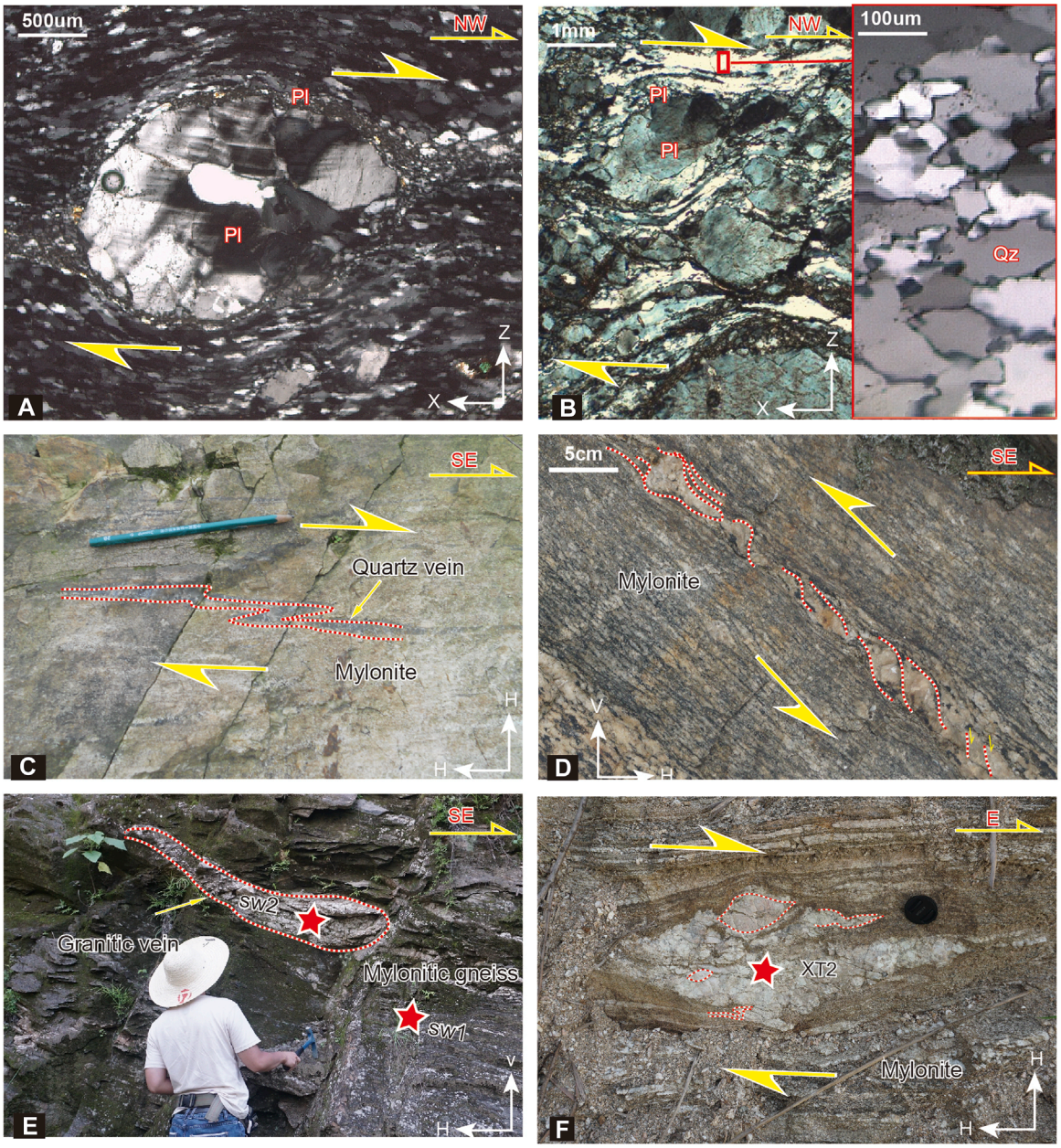

FIGURE 6
Structural features of the SXTSZ. **(A)** A σ-type feldspathic porphyroclast and its BLG recrystallization to form a mantle in the mylonite of SXTSZ, indicating top-to-the-WNW shearing. **(B)** σ-type feldspathic porphyroclasts and GBM recrystallization of quartz on the rims of the porphyroclast. **(C)** A zigzag syn-kinematic quartz vein showing a dextral shearing (top-to-NW) on the Xishui-Tuanfeng segment of the SXTSZ. **(D)** σ, δ, and composite types of feldspathic porphyroclasts of the mylonite of the Yingshan-Xishui segment of the SXTSZ showing revers sense of shear. **(E)** A fish-like syn-kinematic granitic vein without interior foliation, indicating a later-stage injection and a top-to-NW sense of shear, on the Shuihou-Wuhe segment of the SXTSZ. **(F)** A felsic boudinage derived from a syn-kinematic dyke on the Xishui-Tuanfeng segment of the SXTSZ. The oriented feldspathic mega-crystals and the quarter folds on the up-right and lower-left corners consistently indicate top-to-the-NW movements. Photomicrographs are taken under cross polarized light. Abbreviation of the minerals and arrows on the corners of the photos keep the same connotations with those in Figure 4.

dykes occur parallel to the mylonitic foliation, with straight boundaries and foliated borders (Figures 5G,H). Some dykes were injected parallel to the foliation of the country mylonite, and were progressively sheared into asymmetric (Figure 6F) or symmetric (Figure 8C) boudinages. In addition, some fish-shaped felsic veins are sandwiched between mylonitic layers (Figure 6E). These dykes are usually used as ideal chronometers for determining the deformation timing of the shear zones (Hanmer et al., 1997; Brown and Solar, 1998; Ring and Collins, 2005; Boffadossi et al., 2020).

3.2 High-grade basement culmination, three kinematic domains

The inner area of NDC, known as the high-grade basement culmination, serves as the footwall of the inclined mylonitic bounding shear zones. Based on the trajectories of foliation, two dome structures are roughly identified. They are the Luotian dome with a migmatitic core at Huantuling and the Yuexi dome with a migmatitic core near Yanzihe (Figure 2D). Field mapping results demonstrate that both domes generally comprise three types of tectonic lithologies. Their limb areas are dominated by ribbon-striped gneiss (S-L type) at the outer portions and banded gneiss (S>L type) with veined/banded structures at the interior portions, respectively. The core areas mainly dominated by stromatic/layered migmatite (S>>L).

According to their kinematic styles, three flow domains can be identified (Figure 2). The first is the top-to-the-NW non-coaxial flow domain, which corresponds roughly to the ribbon-striped gneissic areas. The second is the NW-SE oriented co-axial dominated flow domain, primarily developed in the banded gneissic areas. The third is the top-to-outward diapiric flow domain that is mainly localized in the stromatic migmatitic areas.

3.2.1 Top-to-the-NW non-coaxial ductile flow domain

Ribbon-striped gneisses at the outer portions of the dome limbs show NW-SE directed non-coaxial ductile flow (Ratschbacher et al., 2000; Faure et al., 2003; Ji et al., 2017). They are characterized by polymineralic quartzo-feldspathic stripes and poly- and mono-crystalline quartz ribbons. Quartz grains in the ribbons generally exhibit straight boundaries and rectangular shapes (Figure 7A).

The mineralogical phase and deformation fabrics in the ribbon-striped gneiss demonstrate relatively higher temperature conditions of approximately 530°C–600°C compared to those in the mylonitic bounding shear zones. This is evidenced by the presence of mineral assemblages of amphibole + biotite + plagioclase, and high-grade mineral shape fabrics such as feldspar fish (Figure 7B) and independent GBM recrystallization of quartz grains. In addition, the dominant operation of prism <a> slip for the deforming quartz, as indicated by the crystallographic fabric of quartz C-axis, further support the higher temperature conditions for this non-coaxial flow (Ratschbacher et al., 2000; Law, 2014; Wang et al., 2018).

Lineations in this domain predominantly have a plunging direction towards the northwest and southeast. The kinematic indicator for this flow universally indicates a top-to-the-NW movement (Figures 7B,C), which is also supported by previous studies (Faure et al., 2003; Lin et al., 2015). The largest granite suite in the North Dabie complex, known as the Tiantangzhai granite complex, exhibits heterogeneous deformation in the hypersolidus state (Deng et al., 2014; Wang et al., 2014) with a similar flow pattern, witnessed by scattered fish-shaped schlierens in the intrusions, indicating top-to-the-NW flowing kinematics (Figure 7D).

3.2.2 NW-SE oriented coaxial dominated plastic flow domain

Into the interior portions of the limb areas, particularly near Luotian and Yanzihe, a NW-SE oriented coaxial flow characterizes the ductile deformation. The rocks have a conspicuous alternation of leucocratic stringers or veins and melanocratic selvedges (Figure 8A), showing a typical band structure. The leucosomes generally consist of plagioclase, K-feldspar, and quartz, while the melanosomes typically consist of biotite, hornblende, and occasionally pyroxene. Monocrystalline quartz ribbons are also widespread in this domain. The quartz ribbons in this domain often exhibit curved boundaries and irregular shapes of larger sizes (Figure 8B). These characteristics suggest a more active grain boundary migration, which can be attributed to higher temperature conditions of upper amphibolite facies (Passchier and Trouw, 2005; Walte et al., 2005).

The foliations are more pronounced than the lineations (S > L) in this domain. The lineations display dominant NW (290°–310°) and SE (110°–130°) plunging directions. Various fabrics at the outcrops and under microscopes predominantly exhibit orthorhombic symmetries on the profile normal to the foliation and parallel to the lineation (Figures 8B,C). A partially foliated granitic dyke, which underwent ductile stretching, is characterized by a symmetric pinch-and-swell structure (Figure 8C). These characters indicate NW-SE oriented coaxial extension in this domain. In addition, some granitic plutons have concordant contact boundaries with the gneissic country rocks, and carry thin deformed carapaces. The foliation and lineation of these carapaces display consistency with those observed in the surrounding country rocks (Figure 8D).

3.2.3 Diapiric submagmatic flow domain

Based on our survey (see Figure 2), we have primarily observed exposed migmatitic cores of the domes in the Huangtuling area and Yanzihe area, restectively. In the Huangtuling area, granulites with mineral assemblages that include orthopyroxene, garnet, hornblende, plagioclase, and ilmenite have been reported (Xia et al., 2003; Chen et al., 2006). Rocks in this domain exhibit high degrees of partial melting and strong compositional segregation, characterized by thicker leucocratic layers at the decimeter scale (generally 10–20 cm). These leucocratic layers contain a higher proportion of K-feldspar compared to other domains. The leucocratic layers alternate with melanocratic layers, primarily consisting of amphibole, biotite, pyroxene, and minor plagioclase (Zhang et al., 2014).

Deformation in this domain is predominantly influenced by sub-magmatic flow, which is characterized by high-temperature crystal plasticity occurring simultaneously with the presence of melt. Migmatitic nebulites and irregular flow folds are easily observed at the outcrops (Figure 9A). In some outcrops, felsic melts fill the cracks of the mafic boudinages (Figure 9B) and accumulatively relocated at the neck zones (Figure 9C), indicating abundant occurrence of melts and melt-enriched embrittment (Walte et al., 2005). Mineral grains are generally automorphic/hypautomorphic and appear to lack crystal plasticity within the grains; quartz aggregates are elongated to form polycrystalline ribbons or sigmoidal shapes but exhibit isohedral triple junctions between individual grains (Figure 9D).

The foliations in this domain are primarily defined by differentiated compositional layering, and in some local cases, by the presence of biotite-rich schlierens (Ji et al., 2017). In contrast, the lineations are much less pronounced (S >> L). They are defined by extended enclaves, stretched felsic veins, alignment

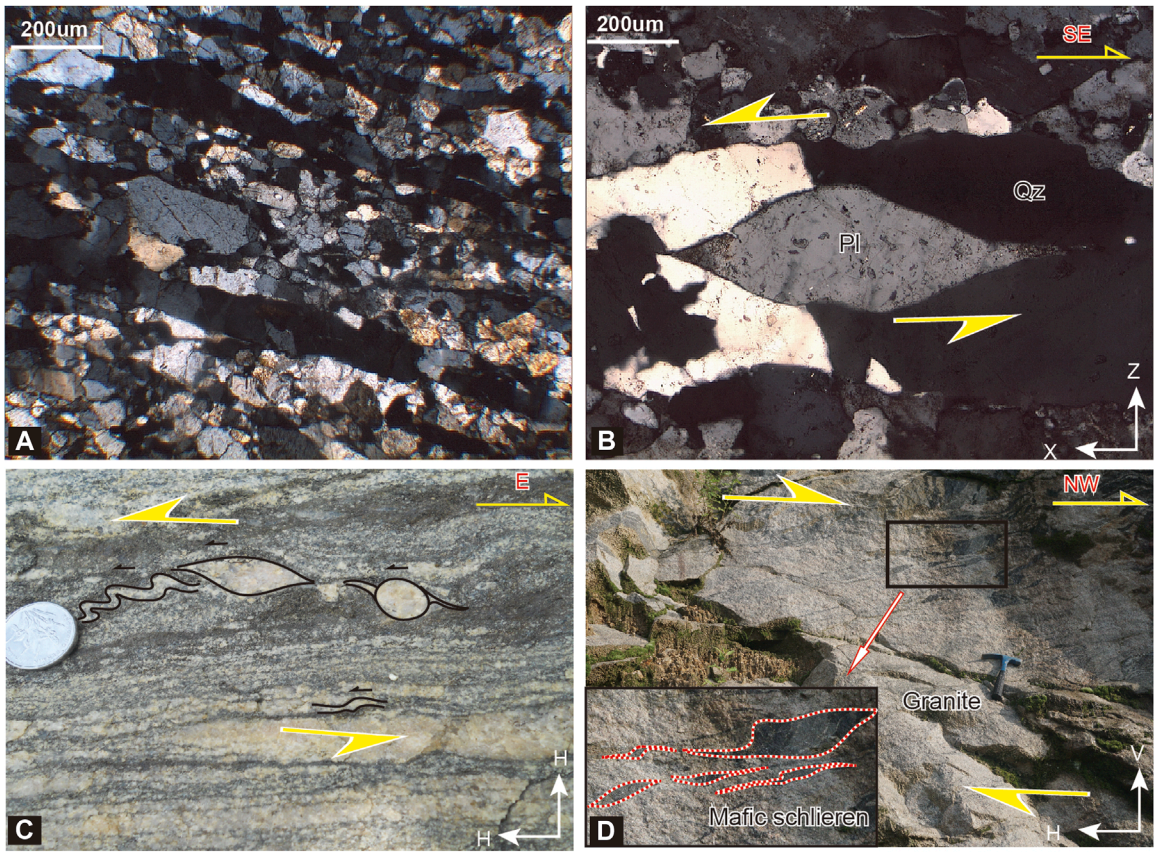

FIGURE 7
Ductile deformation in the non-coaxial dominated domain of the interior of the North Dabie. **(A)** Typical ribbon fabrics defined by elongated poly-and-monocrystalline quartz ribbons with straight boundaries and rectangular shapes. **(B)** Feldspar fish in a quartz ribbon indicating top-to-the-NW motions at high grade conditions. **(C)** Feldspar porphyroclasts of σ-/δ-type and asymmetrically folded felsic veins, appearing to be a sinistral shearing. **(D)** Sheared fish-like mafic schlierens in the Tiantangzhai granite, indicating hypersolidus non-coaxial flow of the intrusion. Photomicrographs are taken under cross polarized light. Abbreviation of the minerals and arrows on the corners of the photos keep the same connotations with those in Figure 4.

of feldspar grains, and elongate aggregates of quartz (if present). These lineations exhibit a radial-directed pattern (Figure 2D). Kinematic structures such as syn-migmatitic normal ductile faults (Faure et al., 1999; Lin et al., 2015; Wang et al., 2018), top-to-downward subsolidus shear bands (Figure 9E), and overturned collapse-style folds (Figure 9F) are observable in the domes. Coupled with the lineation pattern, a top-to-the-outward diapiric fashioned kinematic could hence be inferred for the migmatitic core areas.

4 U-Pb LA-ICP-MS dating of zircon

4.1 Sampling

A total of fifteen samples were collected for U-Pb dating. These samples can be classified into three main categories based on lithology and structural occurrence. The first category consists of mylonite or mylonitic gneiss, banded gneiss, and stromatic migmatite, including samples XMa1, XMa3, SM2, SW1, XT2, YX1, and LT20. The second category comprises granitic dykes, dyke-derived boudins, and intrusive pegmatitic veins, including samples XMa2, SM3, SW2, YX2, XT1, and LT21. The third category is composed of granitic plutons, consisting of samples SM1 and YZ13. Their lithological and structural information are presented in Table 2. Methodology for experiment and data processing is available in supplementary documents.

4.2 Zircon morphology and dating results

Mineral morphology, internal texture, Th/U ratios, and weighted mean $^{206}Pb/^{238}U$ ages of analyzed zircon grains are presented in Table 3. The dating results and detailed description of each sample are presented in the Supplementary documents. Concordia diagrams and representative CL images of the dated zircons are displayed in Figures 10, 11.

A total of 286 concordant ages within the error bars were obtained from the 15 analyzed samples. The ages can be divided into two distinct populations: the Neoproterozoic ranging from 750 Ma to 789 Ma and the Early Cretaceous spanning from 125 Ma to 144 Ma. Neoproterozoic age data were obtained from zircon domains of oscillatory zoning of intact zircon grains (sample XMa1, SM2, SW1, and XT2) and inherited cores (sample XMa3, YX1,

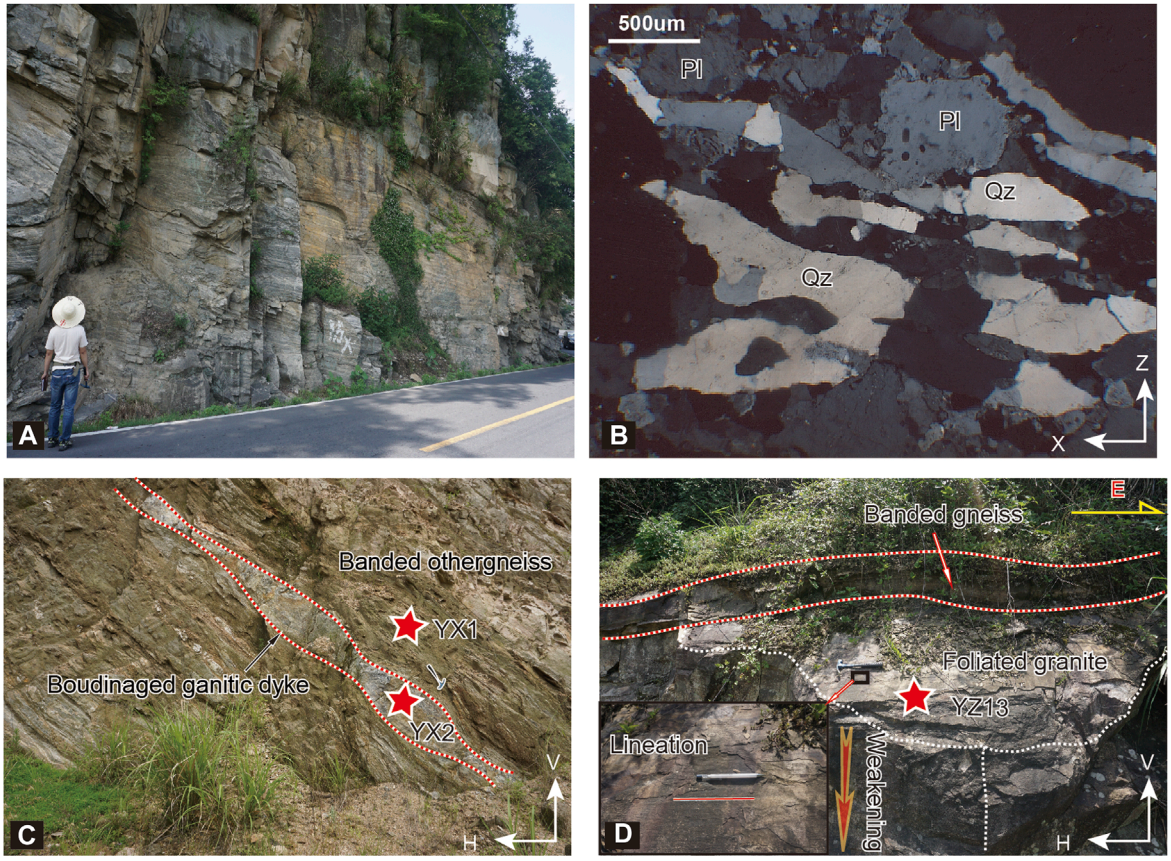

FIGURE 8
Ductile deformation in the banded gneisses of the coaxial dominated flow domain. **(A)** Outcrop of the compositionally differentiated gneissic bands. **(B)** Leucosome of the banded gneiss with curved boundaries and irregular shapes of monocrystalline quartz ribbons. **(C)** Symmetrically boudinaged granitic dyke emplaced parallel with the foliation of the banded orthogneiss. **(D)** Syn-kinematically intruded granitic pluton carrying a deformation carapace with foliation and lineation consistent with those of the country rock. Foliation gradually weakens away from the contact boundary. Photomicrographs are taken under cross polarized light. Abbreviation of the minerals and arrows on the corners of the photos keep the same connotations with those in Figure 4.

and LT20) (Figures 10, 11). Th/U ratios for the analyzed domains range from 0.35 to 1.85. Cretaceous ages dated from felsic mylonite (sample XMa3), granitic plutons (sample SM1 and YZ13), granitic dykes (sample XMa2 and SM3), a felsic vein (sample SW2), granitic boudinages (sample XT2 and XY2), and a granitic pegmatite (sample LT21) are all magmatic in origin for their oscillatory zoning of the internal texture in the analyzed zircons, and relatively high Th/U ratios (>0.2). These ages represent timing of magmatic events (Corfu et al., 2003; Hoskin and Schaltegger, 2003).

All analyzed zircon grains of banded gneiss sample YX1 have a very low and variable Th content of 25–251 ppm and Th/U ratios of 0.01–0.09. Some of them have a core-rim texture, but others do not have core-rim texture with patched or sector zoning or non-zoning. They are likely crystallized from precipitation of metamorphic fluid without breakdown of high Th minerals such as allanite and monazite (Wu et al., 2007b; Rubatto, 2017). They yield a weighted mean $^{206}Pb/^{238}U$ age of 144 ± 2.1 Ma (MSWD = 0.26), representing the timing of fluid-favored metamorphism.

Sample LT20 from a leucosome of stromatic migmatite at Huantuling area yields concordia $^{206}Pb/^{238}U$ ages of 137–127 Ma. All zircons have a weak or distinct oscillatory zoning in CL images (Figure 11). They have a relatively higher and variable Th content of 90–989 and Th/U ratios of 0.31–0.69. These zircon grains are metamorphic origin as well, but they are more likely crystallized from metamorphic melt (Wu et al., 2004 and Wu et al., 2007c; Rubatto, 2017) at higher temperature conditions in which breakdown of Th rich minerals like allanite and monazite occurs. Their ages record the time of extraction and segregation of the felsic melts from the host rocks to form the leucosome.

5 Discussion

5.1 Protolith of the deformed/metamorphic NDC

Previous researchers initially interpreted the NDC as a crustal terrane that was entirely created by Cretaceous extension-related magmatism (Xue et al., 1997; Hacker et al., 1998). This interpretation is mainly supported by Cretaceous zircon ages of the foliated granitoid rocks known as the grey gneisses regionally.

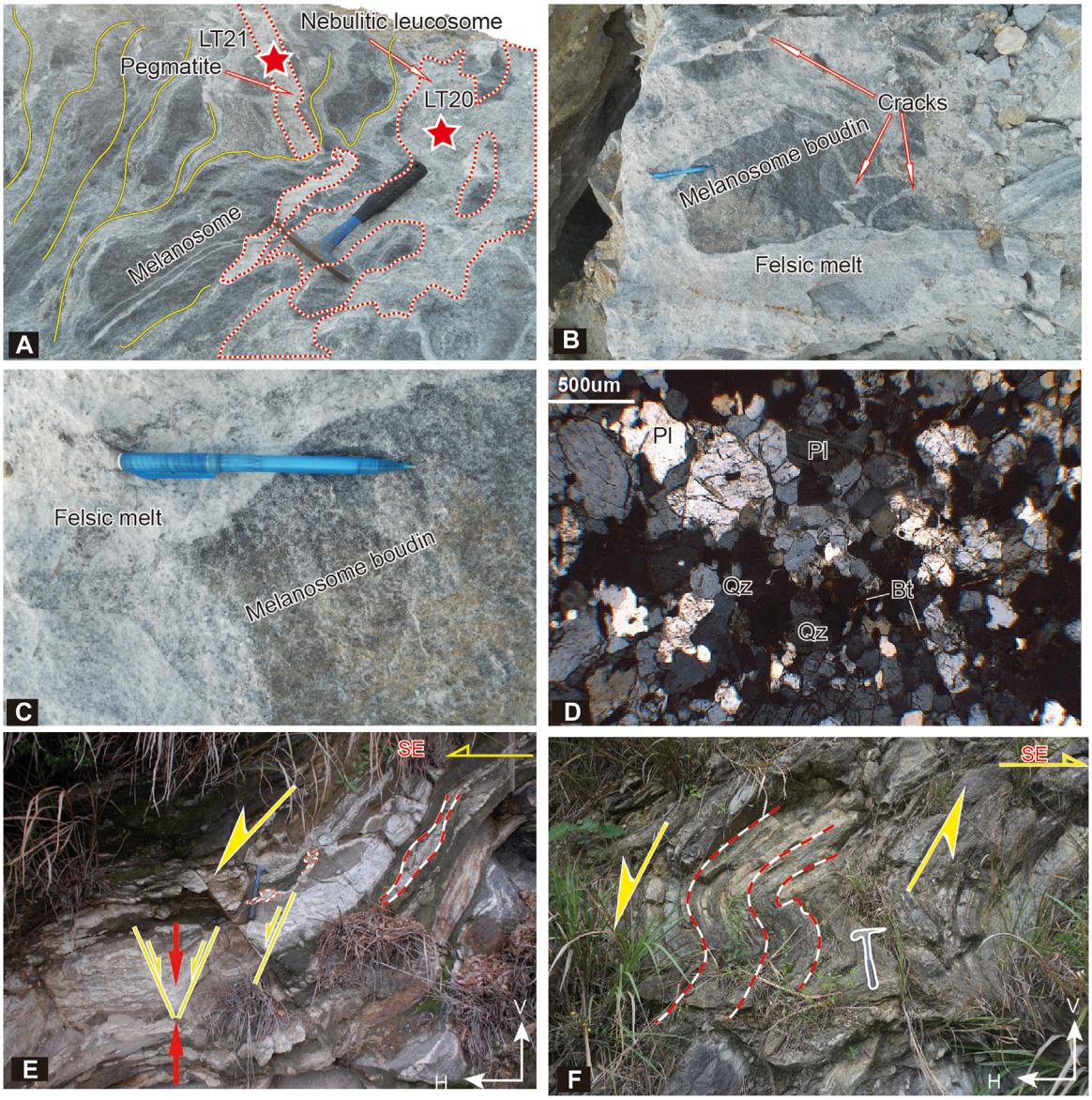

FIGURE 9
Ductile deformation of the migmatites in the diapiric flow domain. **(A)** Highly partial-melted rocks at the core of the migmatitic dome, in which nebulitic leucosome and irregular flow folds are commonly developed. Notice that an undeformed pegmatite intruded into the migmatite. **(B)** Boudinaged melanosome that is cracked inside and with felsic melts filled the cracks. **(C)** Reprecipitation of felsic melts at the low strain site on the corner of the melanosome boudin. **(D)** Micro-fabrics of the leucosome domains of the submagmatic flow in the Niuzhanbi dome. Notice that the mineral grains are slightly strained and weakly oriented, and the quartz grains show isohedral triple junctions. **(E)** Asymmetric ptygmatic folds and sigmoid of winged leucosome, indicating top-to-the-SE collapse. Notice that the conjugate shear bands, demonstrating a nearly layer-perpendicular compression. **(F)** Overturned collapse style fold showing top-to-the-downward kinematics. Photomicrographs are taken under cross polarized light. Abbreviation of the minerals and arrows on the corners of the photos keep the same connotations with those in Figure 4.

However, the specific nature of the ages was not precisely confirmed at that time. Subsequent research provided geochronological evidence suggesting that the majority of the gneisses in this region may originate from Neoproterozoic protoliths, as indicated by the presence of magmatic-type Neoproterozoic ages in most of the dated gneissic rocks (Xue et al., 2002; Bryant, 2004; Liu and Xue, 2007; Zhao et al., 2008; Xie et al., 2010). In addition, a number of Cretaceous ages in the gneisses were proved to be metamorphic in origin (Wu et al., 2007a; Wu et al., 2007b; Yang et al., 2020).

All the deformed/metamorphic rocks (sample XMa1, XMa3, SM2, SW1, XT2, YX1, LT20) performed by LA-ICP-MS zircon U-Pb dating in our study yield Neoproterozoic ages of magmatic in origin. Four samples (XMa1, SM2, SW1, XT2) preserve intact magmatic zircon grains without inherited cores or overgrown rims. They were all collected from mylonitic rocks on the bounding shear zones. The other three samples yield Neoproterozoic ages dated from the inherited magmatic cores, with overgrown rims resulting from metamorphism (YX1 and LT20) and magmatism (XMa3) in the Early Cretaceous, respectively.

Considering the lithological features and comparable age range of orthogneiss in the CDHC and the Luzhengguan Group in the Beihuaiyang belt (Huang et al., 2016; Jiang et al., 2017), we propose that regionally the protolith of the majority of the orthogneiss in North Dabie is similar to those in the Central Dabie and Luzhengguan Group. These Neoproterozoic magmatic rocks are probably formed during rifting of the Rodinia supercontinent (Li et al., 2003; Zheng, 2004; Bader et al., 2013). Locally, some Early Cretaceous magmatites were involved in dynamic metamorphism and associated deformation, such as the sample XMa3.

5.2 Temporal constraints on the deforming NDC

Syn-kinematic plutons typically exhibit a geometric concordance between the country rock and the intrusion margins. Essentially, a fabric gradient is usually observable, transitioning from solid-state deformation at the margins to hypersolidus flow within the intrusion (Ratschbacher et al., 2000; Nzenti et al., 2006; Jolivet et al., 2021). Ductile syn-kinematic dykes are commonly parallel to the pervasive foliation of the country rock, exhibiting foliation along their borders or throughout their entire volume. Pinch-and-swell structures, rotation of winged pegmatitic/aplitic inclusions, and intrafolial folding of dykes are additional indicators of syn-kinematic characteristics (Ring and Collins, 2005; Grasemann et al., 2018). Additionally, pervasive precipitation of metamorphic fluid and crystallization of metamorphic melt within the high-grade deforming metamorphic rocks signify syn-kinematic metamorphism (Corona-Chave et al., 2006; Ganzhorn et al., 2014).

Based on the criteria illustrated above, the following features should belong to syn-kinematic intrusions: the granitic dyke with mylonization at the edges in the SMSZ (Figures 7F,G), the granitic vein of a fish-like shape on the Shuihou-Wuhe

TABLE 2 Rock information of the dated samples.

Sample	Location		Locality	Lithology	Mineral assemblage (volume %)						Structural occurrence
	Longitude	Latitude			Py	Amp	Bt	Pl	Mus	Qz	
XMa1	116°37.62′	31°10.89′	Xiaotian-Mozitan shear zone	mylonite		10	4	55	2	28	sheath fold of mylonitic S-L tectonite
XMa2	116°37.62′	31°10.89′		granite		2	1	58	3	35	dyke cutting across the sheath fold
XMa3	116°02.31′	31°26.40′		felsic mylonite			1	50	3	45	mylonitic S-L tectonite
SM1	115°19.70′	31°32.46′	Shangcheng-Macheng shear zone	granite		1		63	1	34	undeformed pluton intruding into the mylonite
SM2	115°07.53′	31°10.03′				1	5	50	2	40	mylonitic S-L tectonite
SM3	115°07.53′	31°10.03′		granite		1	1	65	2	30	dyke with mylonization at the edges
SW1	116°9.07′	30°49.94′	Shuihou-Xishui-Tuanfeng shear zone	felsic mylonitic				60		35	mylonitic S-L tectonite
SW2	116°9.07′	30°49.94′		granite		2	1	65	1	30	a fish-like vein sandwiched in the mylonite
XT1	115°12.81′	30°28.57′		granite		5	2	60	1	31	felsic boundin with oriented augen feldspar porphyroblasts of σ-type
XT2	115°12.81′	30°28.57′		felsic mylonite				60		35	mylonitic S-L tectonite

(Continued on the following page)

TABLE 2 (*Continued*) Rock information of the dated samples.

Sample	Location		Locality	Lithology	Mineral assemblage (volume %)						Structural occurrence
	Longitude	Latitude			Py	Amp	Bt	Pl	Mus	Qz	
YX1	115°33.90′	30°45.05′	Coaxial flow domain	banded gneiss	1	20		50		28	S>L tectontie, veined/banded
YX2	115°33.90′	30°45.05′		granite		1		60	10	28	symmetrically boudinaged dyke with weak foliation
YZ13	115°58.74′	31°9.36′		granite		1	1	60	2	35	granitic intrusion with deformed carapace
LT20	115°24.18′	30°49.78′	Diapiric flow domain	leucosome of stromatic migmatite				65	1	33	S>>L tectonite, compositionally layered, irregularly folded
LT21	115°24.18′	30°49.78′		pegmatite				65		34	undeformed and emplaced in the country rock

Abbreviations: Py–pyroxene; Amp–amphibolite; Bt–biotite; Mus–muscovite; Qz–quartz.

segment of the SXTSZ (Figure 6E), the delta-shaped felsic boudinage with oriented augen feldspar porphyroblasts on the Xishui-Tuanfeng segment of the SXTSZ (Figures 6F,G), the geometrically symmetric granitic boudinage with weakly foliated edges (Figure 8C), the granitic pluton carrying a foliated carapace (Figure 8D), and the foliated large Tiantangzhan granite complex (Figure 7D). In addition, the banded gneiss (Figure 8C) and nebulitic leucosome (Figure 9A) are interpreted as syn-kinematic metamorphic rocks. The protoliths of the granitic mylonites (Figure 4F; Figure 5F; Figure 6E) are considered as the pre-kinematic intrusions, while the granitic dykes and plutons (Figure 4F; Figure 5E) and pegmatite (Figure 9A) that did not experience ductile deformation are classified as post-kinematic intrusions.

According to the analysis elaborated above, the ductile deformation timing of the XMSZ is suggested to occur after the crystallization of its protoliths, which have been dated as 750.4 ± 7.4 and 142.1 ± 1.4 Ma, respectively. Furthermore, it is proposed to have occurred before the intrusion of the undeformed granitic dyke, dated at 129.4 ± 1.7 Ma, which is consistent with the oldest undeformed plutons reported in the shear zone in a previous study (Wang et al., 2011). Considering the previously reported hornblende $^{40}Ar/^{39}Ar$ ages (Wang et al., 2011), the age of 132 Ma is likely to be synkinematic, while the ages of 127 and 128 Ma likely represent subsequent heating reset ages. The age of 142 Ma is consistent with zircon ages produced in this study and probably represents the crystallization timing of the Early Cretaceous granitic protolith, which survived the later magmatic reheating.

The ductile deformation timing of the SMSZ can be constrained to occur after the protolith age of 743 ± 9.0 Ma and prior to 129.0 ± 1.4 Ma, which is the oldest lower bound reported for undeformed intrusions in the shear zone (Wang et al., 2007 and references therein). Considering the syn-kinematic crystallization age of 136.5 ± 1.7 Ma and hornblende $^{40}Ar/^{39}Ar$ age of ca. 131 Ma (Ji et al., 2017), the ductile deformation timing of the SMSZ is likely to be in the Early Cretaceous and prior to 129 Ma.

Similarly, the ductile deformation of the WXTSZ took place as early as 136.1 ± 1.4 Ma and lasted to 132.0 ± 1.6 Ma in the Early Cretaceous, both of which are syn-kinematic crystallization ages. The oldest undeformed granitic pluton that intruded the mylonitic shear zone was dated as 129 ± 0.8 Ma (Wang et al., 2018), indicating the cessation of the ductile shearing.

In the ribbon-striped gneissic areas, where top-to-the-NW non-coaxial plastic flow dominates the deformation, the syn-kinematic Tiantangzhai granite complex yields LA-ICP-MS and SHRIMP zircon U-Pb ages of 139 ± 3 to 131 ± 4 Ma for the intrusion (Deng et al., 2014). Wu et al. (2007a) obtained SHRIMP zircon U-Pb age of 137 ± 4 Ma for precipitation of the metamorphic fluid in the striped gneisses. In contrast, the ductilely undeformed Zhubuyuan and Baimajian granites intruded into the North Dabie metamorphic complex during 117 ± 11 to 130 ± 3 Ma (Zhao et al., 2004; Wang et al., 2007; Xu et al., 2007; Zhao et al., 2007). These results demonstrate that the non-coaxial flow in this domain commenced as early as 139 Ma and terminated before 130 Ma.

In the banded gneissic areas, where NW-SE oriented coaxial plastic flow controlled the deformation, the syn-kinematically boudinaged dyke in the southern Luotian area yields crystallization

TABLE 3 Zircon information and dating results of the dated samples.

Sample	Morphology		Texture			Th/U			Age (Ma)		
	Size (um)	Shape	With-relict core		Without-relict-core	With-relict core		Without-relict-core	With-relict core		Without-relict-core
			Core	Rim	Intact grain	Core	Rim	Intact grain	Core	Rim	Intact grain
XMa1	100~150	euhedral prism			OZ			0.35~1.49			750.4 ± 7.4
XMa2	50~150	euhedral-subhedral prism			OZ			0.40~1.15			129.4 ± 1.7
XMa3	100~150	euhedral prism	weak OZ	OZ	OZ	0.87~1.17	0.12~2.19		763 ± 28	142.1 ± 1.4	
SM1	100~150	euhedral prism			OZ			0.53~1.15			129.0 ± 1.4
SM2	70~150	euhedral-subhedral prism			OZ			0.39~1.85			742.0 ± 9.0
SM3	30~120	euhedral prism			OZ			0.27~1.07			136.5 ± 1.7
SW1	80~200	euhedral prism			OZ			0.60~1.53			785.2 ± 8.0
SW2	50~150	euhedral-subhedral prism			OZ			0.03~0.10			132.0 ± 1.8
XT1	30~150	subhedral-euhedral prism			OZ			0.01~1.0			136.1 ± 1.4
XT2	80~100	euhedral prism			OZ			0.56~157			789.4 ± 8.1
YX1	40~120	subhedral-anhedral prism	OZ	NZ	NZ, PZ, SZ	0.6~1.81	0.006~0.089		734 ± 24	143.6 ± 2.1	
YX2	30~100	euhedral prism			OZ			0.30~1.0			138.6 ± 1.8
YZ13	100~150	euhedral prism			OZ			0.90~1.5			139.9 ± 1.5
LT20	100~150	anhedral-euhedral prism	OZ	PZ, WZ, OZ		0.90~1.20	0.30~0.70		744 ± 36~812 ± 38	137 ± 2~127 ± 1	
LT21	70~150	anhedral-euhedral prism	OZ	OZ	weak to clear OZ		0.09~0.62			124.7 ± 2.0	

Abbreviations: OZ, oscillatory zoning; NZ, non-zoned; PZ, planer zoning; WZ, weak zoning; SZ, sector zoning; notice the data between rim and intact grain are combination of both.

age of 138.6 ± 1.8 Ma, while the syn-kinematically foliated pluton in the northern Yanzihe area is dated as 139.9 ± 1.5 Ma. In addition, 143.6 ± 2.1 Ma syn-kinematic precipitation of metamorphic fluid in the southern Luotian area corresponds to the same metamorphic process taking place at 140 ± 2 to 138 ± 2 in the northern Yanzihe area (Wu et al., 2007b). These results collectively suggest that the NW-SE oriented coaxial dominated middle-lower crustal flow occurred during ca.144 ~ 138 Ma.

10.3389/feart.2024.1354317

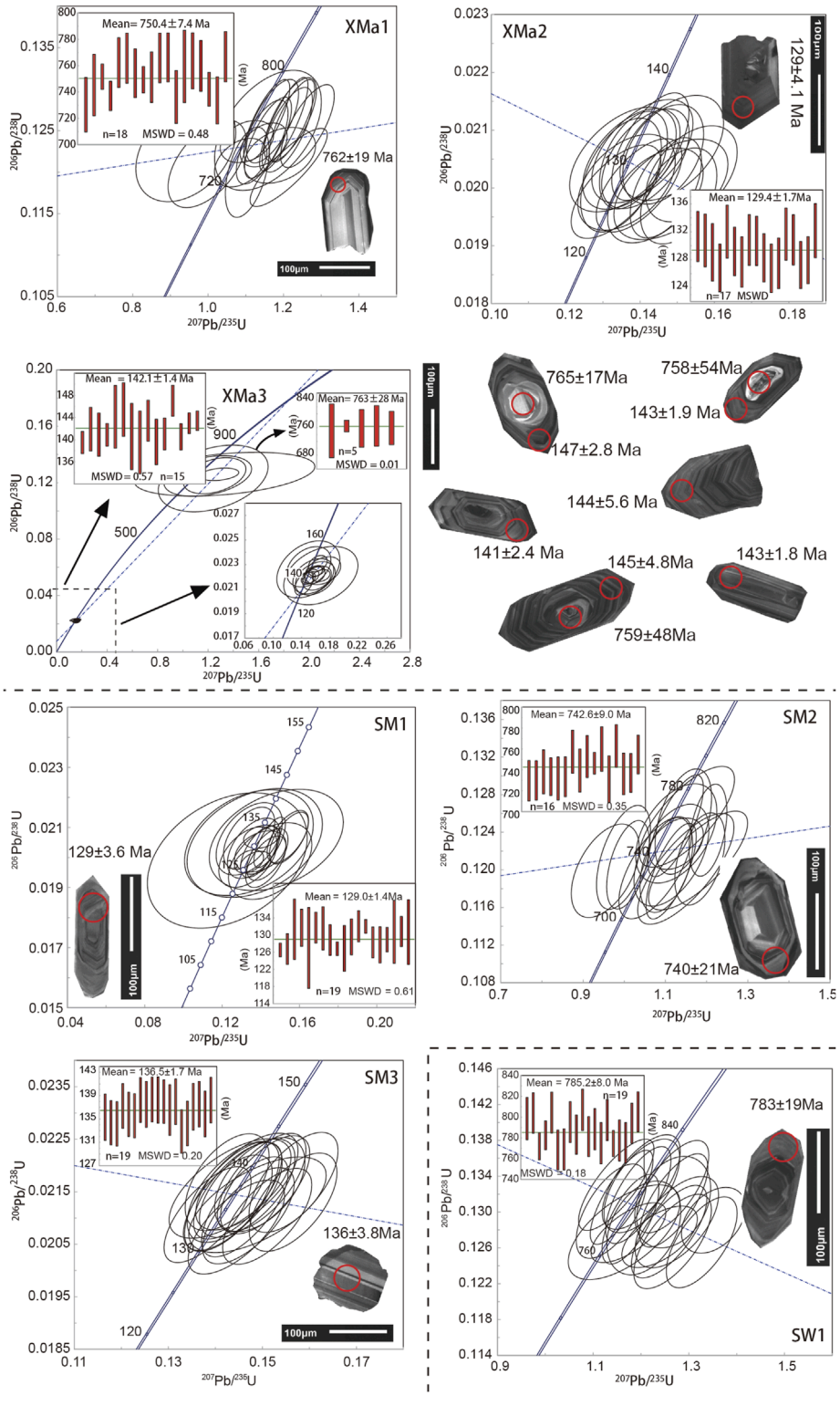

FIGURE 10
Zircon U-Pb concordia diagrams, age spectrum and representative cathodoluminescence (CL) images of zircon grains from the dated samples in the XMSZ (XMa1, XMa2 and XMa3), the SMSZ (SM1, SM2 and SM3), and the SXTSZ (SW1).

The leucosome of the migmatite in the lower/core domain of the southern Hutuling migmatitic dome defines the metamorphic melt activities at 137 Ma to 127 Ma, which is coeval with the 137–129 Ma for migmatites (Wang et al., 2018) in the northern Yanzihe area. In addition, undeformed pegmatite yields a crystallization age of 124.7 ± 2.0 Ma in our study.

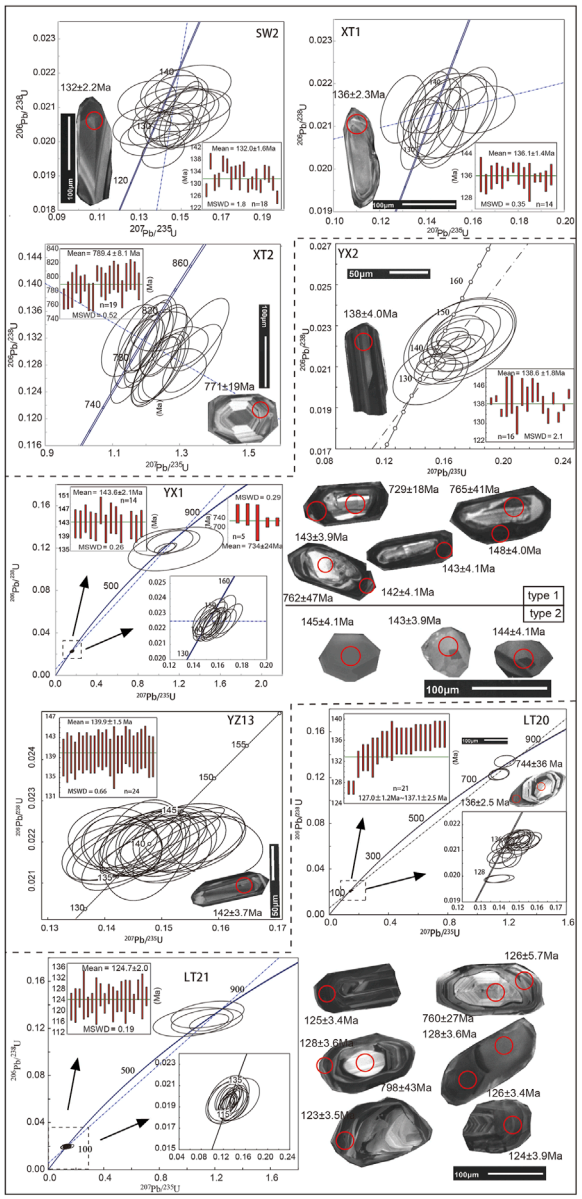

FIGURE 11
Zircon U-Pb concordia diagrams, age spectrum and representative cathodoluminescence (CL) images of zircon grains from the dated samples in the SXTSZ (SW2, XT1 and XT2), the coaxial flow domain (YX1, YX2 and YZ13), and the diapiric flow domain (LT20 and LT21).

These results demonstrate that diapiric-style submagmatic flow in the North Dabie probably took place during ca. 137–125 Ma.

The closure temperature of the $^{40}Ar/^{39}Ar$ system in biotite is constrained to 310°C ± 40°C (Harrison et al., 1985; Grove and Harrison, 1996; Oriolo et al., 2018). At this temperature range, felsic rocks deform sub-ductilely in common geological situations, with quartz exhibiting plastic behavior and feldspars deforming in a brittle manner (Passchier and Trouw, 2005; Fossen, 2016). Biotite $^{40}Ar/^{39}Ar$ ages therefore serve as reliable measure for timing of the sub-ductile deformation. Mylonites in the XMSZ yielded biotite $^{40}Ar/^{39}Ar$ ages of 123 Ma and 121 Ma (Y Wang et al., 2011), consistent with ages of 126–124 Ma of the SXTSZ (Ratschbacher et al., 2000; Hou et al., 2007; Lin et al., 2015; Ji et al., 2017). A syn-kinematically boudinaged granitic pegmatite in the secondary sub-ductile shear zones of the SMSZ yielded a crystallization timing of 126 ± 4.2 Ma (Wang et al., 2007). These age data (Figure 12) demonstrate that the three bounding shear zones successively evolved into a ductile-brittle regime and experienced sub-ductile deformation during ca.130~120 Ma. Analyzed K-feldspar age spectra in the North Dabie complex indicate an overall cooling of the metamorphic complex at ca. 200°C during ca. 120 Ma. This implies that the North Dabie metamorphic complex uplifted into a brittle regime from that point onwards (Chen et al., 1995; Eide et al., 1994; Hacker et al., 1995; Hacker et al., 2000; Ji et al., 2017; Ratschbacher et al., 2000; Wang et al., 2011).

5.3 A composite framework for the early cretaceous extensional tectonics in the NDC

Consistency in deformation is evident across multiple aspects between the bounding mylonitic shear zones, leading to a compelling conclusion. Firstly, a consistent NW-SE directed lineation and a uniform presence of top-to-the-NW/WNW ductile motions are observed within all shear zones, although their strikes and dips are variable. Secondly, through meticulous dating work, we have successfully established the temporal synchronicity of the ductile deformation between these bounding shear zones. Lastly, the thermal conditions of the ductile shearing show remarkable similarities, suggesting a uniform depth of the deformation if assuming a consistent thermal gradient existed at that time. These results demonstrate that these shear zones probably originated from a single, nearly flat-lying shear zone (Lin et al., 2015; Ji et al., 2017).

The NW-SE directed top-to-the-NW/WNW flow not only permeates the mylonites in the bounding shear zones but also extends into the ribbon-striped gneisses of the interior limb areas of the domed metamorphic core complex in the region, during the same geological period. This observation gains further credence when considering the discernible fabric gradient and the scarcity of crosscutting relationships. These results demonstrate that the large-scale shear zone experienced a downward thickening, forming the mylonitic lithologies in the upper part of the middle crust and the gneissic lithologies in the middle part of the middle crust. Consequently, a large-scale detachment processing zone was delineated.

Combining the NW-SE oriented coaxial flow domain occurring in between and the diapiric-styled submagmatic flow domain located at the core, a refined kinematic model can be better established for the North Dabie composite extensional complex. This extensional complex consists of the exhumed HP/UHP rock slices and juxtaposed supra-detachment basins as the rigid upper plate, while the viscously flowing mylonitic-gneissic-migmatitic-magmatic crust acts as the soft

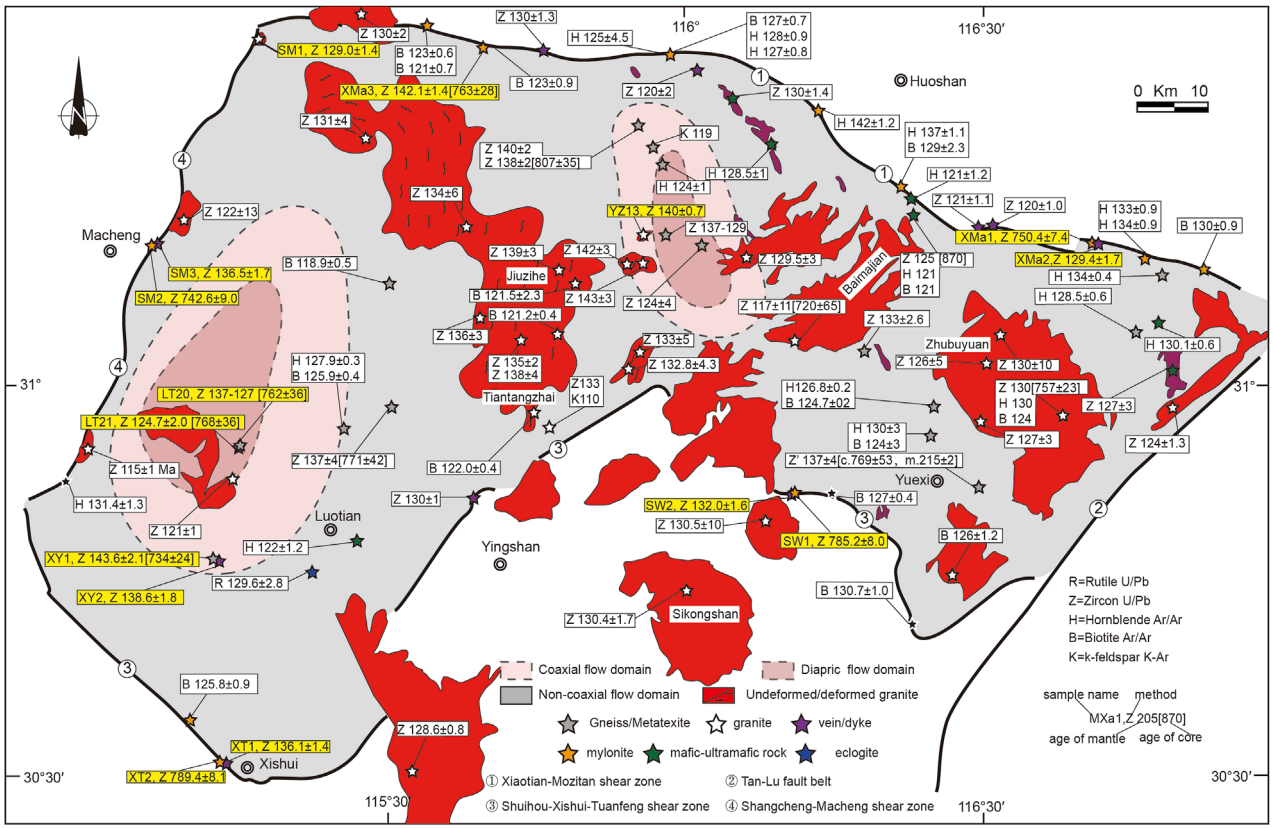

FIGURE 12
Radiometric ages related to the Early Cretaceous thermal events of the North Dabie complex and the bounding shear zones, compiled from previous studies (white boxes) and new data from this study (yellow boxes). Published data are from Chen et al. (1995), Chen et al. (2015), Deng et al. (2014), Eide et al. (1994), Hacker et al. (1995), Hacker et al. (1998), Ji et al. (2017), Lin et al. (2015), Liu and Yan (2020), Liu et al. (2007), Ratschbacher et al. (2000), Wang et al. (2007), Wang et al. (2018), Wang et al. (2011), Wu et al. (2007c), Xu et al. (2002).

lower plate. The upper plate behaves in a brittle manner, whereas the lower plate shows ductile flow in various styles (Figure 13A).

The flowing lower plate exhibits distinct structural characteristics: a large-scale detachment processing zone at the top, a coaxial plastic flow zone in the middle, and a sub-magmatic diapiric uprising flow from below (Figure 13A). The detachment processing zone accommodates intense strain at upper-middle levels of the middle crust (upper greenschist facies to middle amphibolite facies) through top-to-the-NW shearing (Figure 13B). The coaxial plastic flow zone, stretched in the same direction, develops in the middle-lower levels of the middle crust (upper amphibolite facies). The migmatitic subsolidus flow ascends from deeper levels in the lower crust, exhibiting a top-to-outward diapiric kinematic style under the granulite facies conditions. Syn-kinematic melts inject into the flowing rocks, further weakening the crust and enhancing their efficiency of flow. Isostatically driven doming and diapiric flow (inflation and buoyancy) unevenly uplift the detachment processing zones and the coaxial flow zone, resulting in the formation of the North Dabie gneiss-migmatite dome system. When the upper plate is eroded, this uplift exposes them as a metamorphic window. Consequently, the detachment mylonitic zone separates into the Xiaotian-Mozitan shear zone to the north, the Shangcheng-Macheng shear zone to the west, and the curved Shuihou-Xishui-Tuanfeng shear zone to the south and east (Figure 13A).

5.4 Geodynamics and structural evolution for NDC

Post-collisional collapse of the DOB has been widely employed by numerous researchers to explain the Early Cretaceous tectono-thermal event especially the magmatic activities in this period within the DOB (Zhao et al., 2004; Zhao et al., 2005; Zhao et al., 2007; Zhao et al., 2008; He et al., 2011; Li et al., 2013; He et al., 2022). However, the undeformed Jurassic sedimentary rocks unconformably overlie the deformed pre-Triassic rocks in the northern Behuaiyang belt and the southern Yangtze foreland fold-and-thrust belt, indicating the termination of the orogeny prior to the earliest Jurassic. Geochronological data also demonstrate a >100 Ma temporal gap between the initial collision of NCB–SCB during ca. 270–252 Ma and the onset of the Early Cretaceous magmatic activities (ca. 143 Ma). Therefore, it is difficult to link the Early Cretaceous tectono-thermal event with the Late Permian-Triassic orogenic processes.

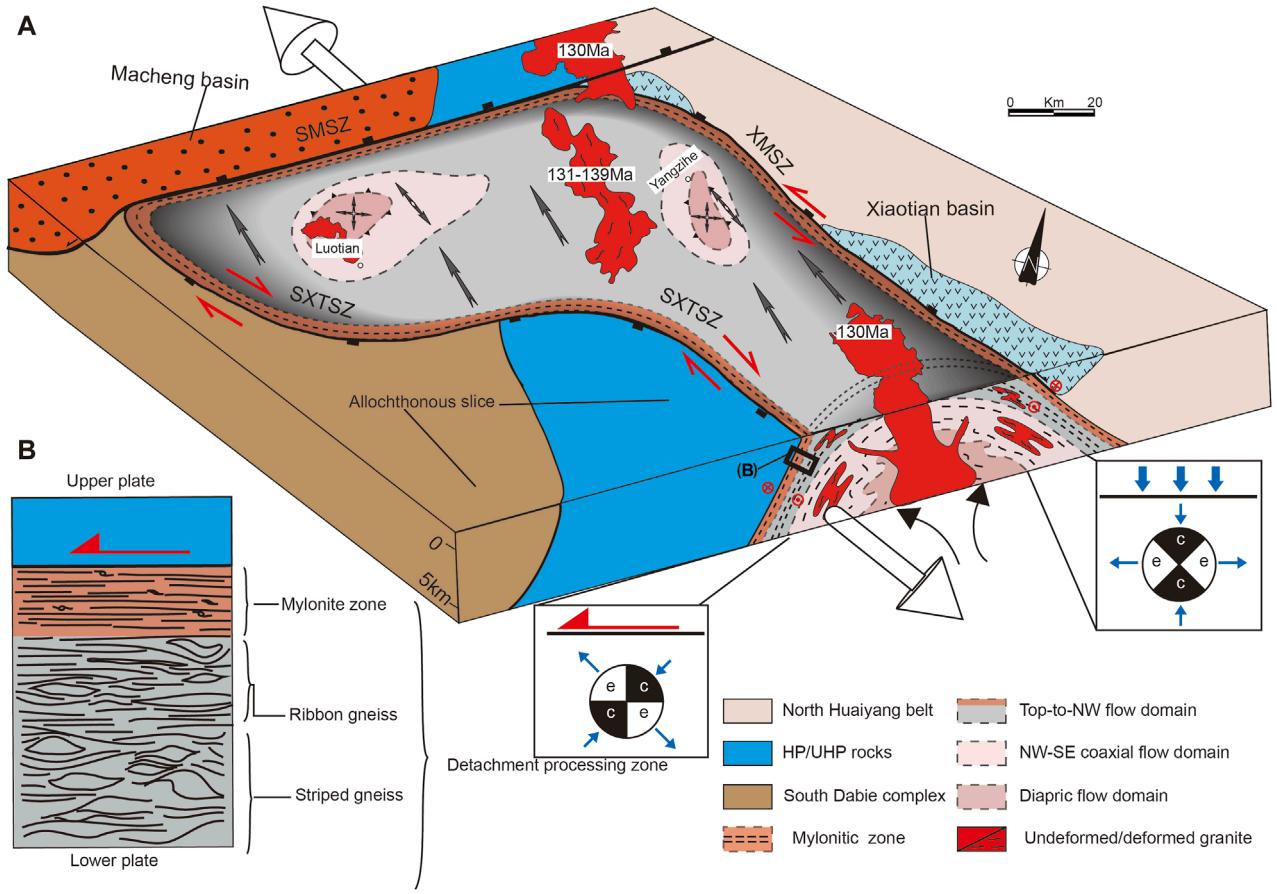

FIGURE 13
(A) Block diagram of schematic structural-kinematic model for the composite extensional complex of the Dabie Early Cretaceous extensional tectonics. **(B)** Fabric gradient of the detachment processing zone. XMSZ = Xiaotian-Mozitan shear zone; SXTSZ = Shuihou-Xishui-Tuanfeng shear zone; SMSZ = Shangcheng-Macheng shear zone; e = instantaneous extensional field; c = instantaneous contractional field.

Considering the tectonic settings of the DOB in the Early Cretaceous, several dynamic factors potentially contributed to this extensional tectonics. A thickened lithosphere with a crust over 50 km thick in the Dabie orogenic belt (He et al., 2011) was formed through a robust continental collision between the North China Block (NCB) and the South China Block (SCB), resulting in significant gravitational instability. To the north, the closure of the Mongol-Okhotsk Ocean caused a large field of contractional regime until the Early Cretaceous (Cogné et al., 2005; Fritzell et al., 2016; Sorokin et al., 2020). To the southwest, the consumption of the Meso-Tethys Ocean along the northern margins of Lhasa-Indosinia (Metcalfe, 2013; Fan et al., 2021; Liu et al., 2022) potentially causes far field compression to the Dabie region. To the east, the paleo-western Pacific plate subducted beneath the East Asian continent accompanied with a widely proposed slab roll-back during this period (Zhu et al., 2017a; Zhu and Xu, 2019).

Regionally, extensional structures, such as MCC type extensional gneissic domes, detachment faults, and extension-related basins, are widespread from Trans-Baikal to SCB, over more than 3,000 km along the eastern Asian continent (Figure 14) (Huang et al., 2021; Lin et al., 2015; Wang et al., 2011; Zhou et al., 2012). These extensional structures exhibit a consistent NW-SE oriented maximum stretching direction. They were predominantly developed during the Early Cretaceous of ca. 140–120 Ma (Lin et al., 2015; and references therein). Obviously, these extensional structures likely share a common geodynamic origin. It is considered that the far-field back-arc extension caused by the northwest-directed subducting paleo-western Pacific plate may contribute the main force to drive the large-scale extension (Lin et al., 2015; Zhu et al., 2017b; Jiang et al., 2017; Li et al., 2019).

Together with the spatiotemporal configuration of the structures and associated metamorphism and magmatism in the NDC, a schematic multi-stage tectono-structural evolution for the extensional deformation is outlined as follows:

(1) Development of NW-SE coaxial flow in the middle-lower crust at 144–138 Ma (Figure 15A)

The exhumed HP-UHP rock slices overlay as a cover of the DOB before the extension started to take place (Hacker et al., 2000; Faure et al., 2003), contributing to substantially thickening of the Dabie lithosphere. As a result, gravitational instability

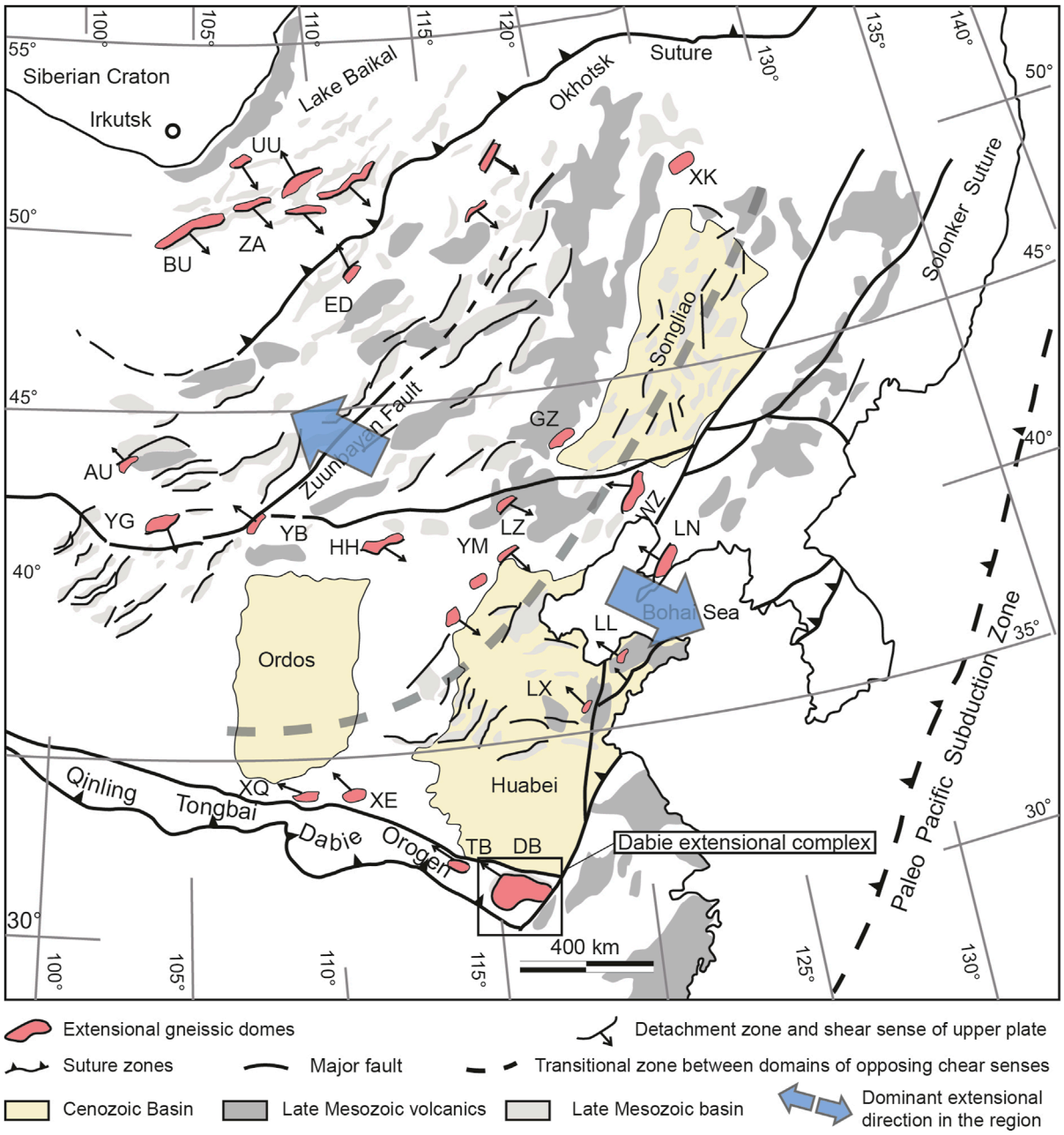

FIGURE 14
Early Cretaceous extensional structures in Eastern Asia (modified after Wang et al., 2011b; Zhou et al., 2012; Lin et al., 2015). Metamorphic gneissic domes include Buteel-Burgutoy (BU), Norh Dabie (DB), Ereendavaa (ED), Hohhot (HH), Linglong (LL), Liaonan (LN), Tongbai (TB), Ulan-Ude (UU), Waziyu or Yiwulvshan (WZ), Yingba (YB), Yagan (YG), Yunmenshan (YM), Xiong'er, XK-Xinkailing (XE), Xiaoqinling (XQ) and Zagan (ZA).

was fostered and eclogitization probably occurred at the bottom of the lower crust (Wang et al., 2007). Strong rollback of the subducting Paleo-Pacific plate and fast trench retreat in the eastern Asia during the Late Jurassic-Early Cretaceous (Meng et al., 2014; Zhu et al., 2017a; Li et al., 2019) likely induced a significant change in tectonic regime for the DOB from N-S direction dominated contraction into NW-SE direction dominated extension/transtension.

In light of these circumstances, it is evident that the lithosphere of the DOB experienced a significant phase of NW-SE-directed coaxial-dominated flow within the coherent middle-lower crust. This flow began at ca. 144 Ma and lasted to ca. 138 Ma, marking the initiation of the regional extension. This crustal flow introduced fluctuations into the highly active, non-equilibrium orogenic system of the DOB. This dynamic process also facilitated mobility of metamorphic fluids and locally triggered decompression-related

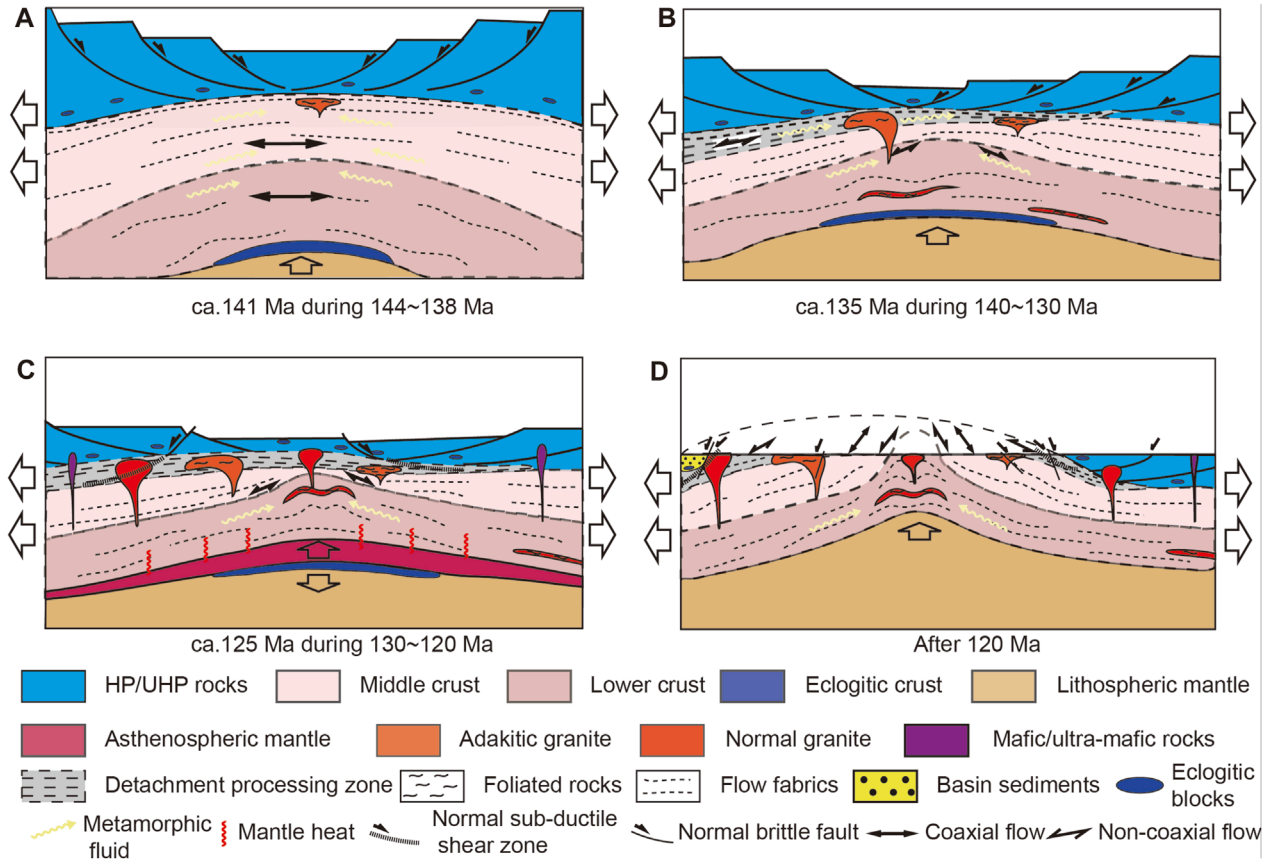

FIGURE 15
Conceptual block diagrams showing tectono-structural evolution of the Dabie Early Cretaceous extensional tectonics. Care should be taken that arrows in the rocks indicate active state of the deformation, while those without arrows means "freezing in" of the previously active deformation. **(A)** NW-SE oriented coaxial flowing in the middle-lower crust; **(B)** Top-to-the-NW non-coaxial flowing in the detachment processing zone and uprising sub-magmatic flow from the lower crust; **(C)** Transtensional sub-ductile overprinting on the detachment; **(D)** Brittle normal faulting superimposition.

adakitic melts, which originated from the eclogitic bottom of the lower crust.

(2) Formation of the detachment processing zone and initiation of migmatitic diapric flow at 140–130 Ma (Figure 15B)

The emplacement of adakitic granites heterogeneously softened the crust in the middle levels. As a result, regional extension was primarily localized into the weakened upper-middle part of the middle crust, giving rise to the development of a large-scale detachment processing zone. Deformation of the zone likely initiated around 140 Ma, slightly later than the onset of the magmatic activities (Ca. 143 Ma according to Wang et al., 2007). This zone accommodated the extensional strain by means of top-to-the-NW/NWW non-coaxial ductile flow, which lasted to ca. 130 Ma.

Structural weakening during the detachment processing enhanced permeability of the deformation domain (Fossen and Cavalcante, 2017), and made it an effective channel path for crustal melts to transfer (Brown and Solar, 1998; Jolivet et al., 2021). The syn-kinematic Tiantangzhai granite complex was arrested during this course.

Pervasive micro-mesoscopic partial melting and perlocative flow of the melts within the migmatites in the lower crust induced decrease of its density and viscosity (Gilbert and Merle, 1987; Rey et al., 2009). These changes prompted rheological instability, which further initiated a diapiric flow of the migmatitic lower crust (Yin, 2004) at ca. 137 Ma. Radial stretching lineations and top-to-outward kinematics characterized this flow.

The detachment-related arching and the diapric flow induced differential uprising incrementally domed the region; isostatic-rebound caused by the extensional thinning increasingly uplift the metamorphic lower plate up to higher levels.

(3) Heterogeneous doming inside and uniform uplift along the bounding shear zones at 130–120 Ma (Figure 15C)

The extraction of melts from the eclogitic bottom of the lower crust persistently increases its density, which ultimately triggered mantle delamination (Zhao et al., 2007; He et al., 2011; Xu et al., 2012; Li et al., 2013; Zhang et al., 2015; Li et al., 2021). This allowed upwelling mantle to pump mafic-ultramafic magma up into the crust, and to heat the lower crust to produce normal granites.

Magmatic activities reached the peak at this stage. The powerful magma inflation and forceful buoyancy heterogeneously uplifted the detachment processing zone and the metamorphic complex beneath it. Consequently, the dome-shaped zone wrapped the gneiss-migmatite core, with its roof part covering the core and the wall part surrounding the core.

Meanwhile, incremental localization of the extensional strain resulted in networks of outcrop-scale strike-slip-normal sub-ductile shear zones that primarily overprinted on the tilted wall part of the detachment processing zone. This structural style accounted for a uniform uplift of the entire North Dabie metamorphic complex to a higher level of approximately 6–7 km (200 °C) in the upper crust around 120 Ma. During the same process, this sub-ductile shearing separated the roof part of the dome-shaped detachment from its wall part, and progressively split the initially continuous wall part into different segments–the rudiments of the individual bounding shear zones.

(4) Thinning by superposition of normal brittle faulting after 120 Ma (Figure 15D)

Dwindling of magmatism after 120 Ma in the Dabie orogen (Xu et al., 2002; Wang et al., 2007) coincides with the shallowing dip of the westward-subducting Paleo-Pacific plate (Zhu et al., 2017a). Intensity of the extensional deformation probably decreased, which is indicated by a slow-down of the uplift speed of the North Dabie metamorphic complex after this time (Wang et al., 2014). Normal brittle faulting superposed on the metamorphic complex. This brittle deformation in particular enhanced activity of the already superposed bounding shear zones, and transferred them into major normal faults that controlled the growth of the detachment-related basins such as the Xiaotian basin to the north and the Macheng basin to the west (also Figure 12). The exhumed HP/UHP slices served as considerable sedimentary sources to feed the basins. This is evidenced by Triassic aged zircon grains found in the Early Cretaceous sediments and volcanic rocks on the north foot of the Dabie Mountains (Zhu et al., 2017b).

As denudation continuously took place, the mylonites in the roof part of the arched detachment were removed; the ribbon-stripped gneisses, banded gneisses and migmatites were consequently exposed in the metamorphic window. The separated segments which were originated from the wall part of the detachment are finally located individually around the metamorphic window, as the Xiangtian-Mozitan shear zone to the north, the Shangcheng-Macheng shear zone to the west, and the Shuihou-Xishui-Tuanfeng shear zone to the east and south.

6 Conclusion

(1) The current tilted bounding shear zones that confine the North Dabie high-grade basement culmination are likely derived from an initially flat-lying single detachment processing zone, which developed during ca. 140–130 Ma through top-to-the-NW/WNW shearing.
(2) A NW-SE oriented coaxial dominated plastic flow at the middle-lower crust developed during ca.144~138 Ma, indicating the initiation of the Early Cretaceous extension and the precursor of the detachment formation.
(3) A sub-magmatic flow actively ascended from the lower crust during ca. 137–125 Ma in a diapiric manner to form the migmatitic cores of the North Dabie gneiss-migmatite domes.
(4) The Dabie deep crust underwent a successive multi-stage extensional deformation and uplifting during the Early Cretaceous extension, from coaxial dominated plastic flow in the middle-lower curst to non-coaxial ductile shearing localized in the middle crust, and diapiric sub-magmatic flow rising from the deeper lower crust to uniform uplift by transtensional sub-ductile shear zones, and to brittle normal faults overprinting at the end.

Data availability statement

The original contributions presented in the study are included in the article/Supplementary Material, further inquiries can be directed to the corresponding authors.

Author contributions

PH: Conceptualization, Data curation, Formal Analysis, Funding acquisition, Investigation, Methodology, Project administration, Resources, Writing–original draft. ZY: Writing–review and editing. WX: Conceptualization, Formal Analysis, Funding acquisition, Investigation, Project administration, Supervision, Writing–review and editing. MS: Formal Analysis, Investigation, Methodology, Resources, Writing–original draft. QM: Formal Analysis, Funding acquisition, Project administration, Supervision, Writing–original draft, Writing–review and editing. NA: Conceptualization, Formal Analysis, Methodology, Writing–review and editing.

Funding

The author(s) declare financial support was received for the research, authorship, and/or publication of this article. The study was financially supported by the National Natural Science Foundation of China (Nos. 42002230; U2003107), the Science and Technology Major Project of Xinjiang Uygur Autonomous Region, China (2021A03001-1and4, 2022A03010-1), One Hundred Talent Program of the Chinese Academy of Sciences (E2250403), Youth Innovation Promotion Association Chinese Academy of Sciences (2022446). This is a contribution to IGCP 662.

Acknowledgments

We sincerely thank Daoxuan Wang, Hailong Li and Yangyang Wang for their help in our field work. We would like to also show our gratitude to Quanzhong Li and Xiaoqiang Liu for their support in zircon U-Pb analysis. A special acknowledgment is expressed

to China-Pakistan Joint Research Centre on Earth Sciences that supported the implementation of this study. Data supplementing this paper are available in the Supplementary Material from Supplementary one to five.

Conflict of interest

The authors declare that the research was conducted in the absence of any commercial or financial relationships that could be construed as a potential conflict of interest.

The author(s) declared that they were an editorial board member of Frontiers, at the time of submission. This had no impact on the peer review process and the final decision.

Publisher's note

Supplementary material

The Supplementary Material for this article can be found online at: https://www.frontiersin.org/articles/10.3389/feart.2024.1354317/full#supplementary-material

References

Albertz, M. (2006). Relationships between melt-induced rheological transitions and finite strain: observations from host rock pendants of the Tuolumne Intrusive Suite, Sierra Nevada, California. *J. Struct. Geol.* 28 (8), 1422–1444. doi:10.1016/j.jsg.2006.04.001

Ames, L., Zhou, G., and Xiong, B. (1996). Geochronology and isotopic character of ultrahigh-pressure metamorphism with implications for collision of the Sino-Korean and Yangtze cratons, central China. *Tectonics* 15 (2), 472–489. doi:10.1029/95TC02552

Ávila, C. F., Archanjo, C. J., Fossen, H., and Hollanda, M. H. B. M. (2019). Zippered shear zone model for interacting shear zones in the borborema province, Brazil, as constrained by U-Pb dating. *U-Pb Dating* 38 (11), 3959–3974. doi:10.1029/2019TC005547

Ayers, J. C., Dunkle, S., Gao, S., and Miller, C. F. (2002). Constraints on timing of peak and retrograde metamorphism in the Dabie Shan Ultrahigh-Pressure Metamorphic Belt, east-central China, using U–Th–Pb dating of zircon and monazite. *Chem. Geol.* 186 (3), 315–331. doi:10.1016/S0009-2541(02)00008-6

Bader, T., Ratschbacher, L., Franz, L., Yang, Z., Hofmann, M., Linnemann, U., et al. (2013). The heart of China revisited, I. Proterozoic tectonics of the Qin mountains in the core of supercontinent Rodinia. *Proterozoic Tect. Qin Mt. core supercontinent Rodinia* 32 (3), 661–687. doi:10.1002/tect.20024

Boffadossi, M., Coniglio, J., Maffini, M., Pinotti, L., Radice, S., D'Eramo, F., et al. (2020). Synkinematic interplay between felsic dykes and host rock mylonitization: how magmatism assists the formation of ductile narrow shear zones in the Sierra Chica de Córdoba, Argentina. *J. S. Am. Earth Sci.* 106, 103063. doi:10.1016/j.jsames.2020.103063

Brown, M., and Solar, G. S. (1998). Shear-zone systems and melts: feedback relations and self-organization in orogenic belts. *J. Struct. Geol.* 20 (2), 211–227. doi:10.1016/S0191-8141(97)00068-0

Bryant, D. L., Ayers, J. C., Gao, S., Miller, C. F., and Zhang, H. (2004). Geochemical, age, and isotopic constraints on the location of the sino-Korean/Yangtze suture and evolution of the northern dabie complex, east Central China. *Geol. Soc. Am. Bull.* 116 (5), 698–717. doi:10.1130/B25302.2

Bucher, K. (2023). *Petrogenesis of metamorphic rocks*. Cham: Springer International Publishing.

Carswell, D. A., Wilson, R. N., and Zhai, M. (2000). Metamorphic evolution, mineral chemistry and thermobarometry of schists and orthogneisses hosting ultra-high pressure eclogites in the Dabieshan of central China. *Lithos* 52 (1), 121–155. doi:10.1016/S0024-4937(99)00088-2

Chen, F., Guo, J.-H., Jiang, L.-L., Siebel, W., Cong, B., and Satir, M. (2003). Provenance of the Beihuaiyang lower-grade metamorphic zone of the Dabie ultrahigh-pressure collisional orogen, China: evidence from zircon ages. *J. Asian Earth Sci.* 22 (4), 343–352. doi:10.1016/S1367-9120(03)00068-3

Chen, J., Xie, Z., Liu, S., Li, X. M., and Foland, K. (1995). Cooling age of Dabie orogen, China, determined by ^{40}Ar-^{39}Ar and fission track techniques. *Sci. China (Scientia Sinica) Ser. B* 38, 749–757.

Chen, R.-X., Ding, B., Zheng, Y.-F., and Hu, Z. (2015). Multiple episodes of anatexis in a collisional orogen: zircon evidence from migmatite in the Dabie orogen. *Lithos* 212-215, 247–265. doi:10.1016/j.lithos.2014.11.004

Chen, Y., Ye, K., Liu, J.-B., and Sun, M. (2006). Multistage metamorphism of the Huangtuling granulite, Northern Dabie Orogen, eastern China: implications for the tectonometamorphic evolution of subducted lower continental crust. *J. Metamorph. Geol.* 24 (7), 633–654. doi:10.1111/j.1525-1314.2006.00659.x

Cogné, J.-P., Kravchinsky, V., Halim, N., and Hankard, F. (2005). Late jurassic-early cretaceous closure of the Mongol-Okhotsk Ocean demonstrated by new mesozoic palaeomagnetic results from the trans-baïkal area (SE siberia). *Geophys. J. Int.* 163, 813–832. doi:10.1111/j.1365-246X.2005.02782.x

Corfu, F., Hanchar, J., Hoskin, P. W. O., and Kinny, P. (2003). Atlas of zircon textures. *Rev. Mineralogy Geochem.* 53, 469–500. doi:10.2113/0530469

Corona-Chave, P., Poli, S., and Bigioggero, B. (2006). Syn-deformational migmatites and magmatic-arc metamorphism in the Xolapa Complex, southern Mexico. *J. Metamorph. Geol.* 24 (3), 169–191. doi:10.1111/j.1525-1314.2006.00632.x

Deng, X., Yang, K., Polat, A., Kusky, T., and Wu, K. (2014). Zircon U-Pb ages, major and trace elements, and Hf isotope characteristics of the Tiantangzhai granites in the North Dabie orogen, Central China: tectonic implications. *Geol. Mag.* 151 (5), 916–937. doi:10.1017/S0016756813000976

Dong, S., Gao, R., Cong, B., Zhao, Z., Liu, X., Li, S., et al. (2004), Crustal structure of the southern Dabie ultrahigh-pressure orogen and Yangtze foreland from deep seismic reflection profiling. *Terra nova.* 16 (6), 319–324. doi:10.1111/j.1365-3121.2004.00568.x

Dong, Y., and Santosh, M. (2016). Tectonic architecture and multiple orogeny of the qinling orogenic belt, Central China. *Gondwana Res.* 29 (1), 1–40. doi:10.1016/j.gr.2015.06.009

Dong, Y., Sun, S., Santosh, M., Hui, B., Sun, J., Zhang, F., et al. (2022). Cross orogenic belts in Central China: implications for the tectonic and paleogeographic evolution of the East asian continental collage. *Gondwana Res.* 109, 18–88. doi:10.1016/j.gr.2022.04.012

Eide, E., McWilliams, M., and Liou, J. (1994). ^{40}Ar/^{39}Ar geochronology and exhumation of high-pressure to ultrahigh-pressure metamorphic rocks in east-central China. *Geology* 22 (7), 601–604. doi:10.1130/0091-7613(1994)022<0601:AAGAEO>2.3.CO;2

Fan, J.-J., Niu, Y., Liu, Y.-M., and Hao, Y.-J. (2021). Timing of closure of the Meso-Tethys Ocean: constraints from remnants of a 141–135 Ma ocean island within the bangong–nujiang suture zone, Tibetan plateau. *GSA Bull.* 133 (9-10), 1875–1889. doi:10.1130/b35896.1

Faure, M., Lin, W., Shu, L. S., Sun, Y., and Schärer, U. (1999). Tectonics of the Dabieshan (eastern China) and possible exhumation mechanism of ultra high-pressure rocks. *Terra nova.* 11, 251–258. doi:10.1046/j.1365-3121.1999.00257.x

Faure, M., and Lin, W., (1998). Doming in the southern foreland of the Dabieshan (Yangtse block, China). *Terra nova.* 10, 307–311. doi:10.1046/j.1365-3121.1998.00207.x

Faure, M., Schärer, U., Liangshu, S., Sun, Y., and Arnaud, N. (2003). Continental subduction and exhumation of UHP rocks. Structural and geochronological insights from the Dabieshan (East China). *Lithos* 70, 213–241. doi:10.1016/S0024-4937(03)00100-2

Fossen, H. (2016). *Structural Geology*. Cambridge: Cambridge University Press, 16–136.

Fossen, H., and Cavalcante, G. C. G. (2017). Shear zones – a review. *Earth-Science Rev.* 171, 434–455. doi:10.1016/j.earscirev.2017.05.002

Fritzell, E. H., Bull, A. L., and Shephard, G. E. (2016). Closure of the mongol–okhotsk ocean: insights from seismic tomography and numerical modelling. *Earth Planet. Sci. Lett.* 445, 1–12. doi:10.1016/j.epsl.2016.03.042

Ganzhorn, A. C., Labrousse, L., Prouteau, G., Leroy, C., Vrijmoed, J. C., Andersen, T. B., et al. (2014). Structural, petrological and chemical analysis of syn-kinematic migmatites: insights from the Western Gneiss Region, Norway. *J. Metamorph. Geol.* 32 (6), 647–673. doi:10.1111/jmg.12084

Gilbert, E., and Merle, O. (1987). Extrusion and radial spreading beyond a closing channel. *J. Struct. Geol.* 9 (4), 481–490. doi:10.1016/0191-8141(87)90123-4

Grasemann, B., Dabrowski, M., and Schöpfer, M. (2018). Sense and non-sense of shear reloaded. *J. Struct. Geol.* 125, 20–28. doi:10.1016/j.jsg.2018.05.028

Grove, M., and Harrison, T. M. (1996). ^{40}Ar (super ∗) diffusion in Fe-rich biotite. *Am. Mineralogist* 81 (7-8), 940–951. doi:10.2138/am-1996-7-816

Hacker, B., Ratschbacher, L., Webb, L., and Dong, S. (1995). What brought them up? Exhuming the Dabie Shan ultrahigh-pressure rocks. *Geology* 23 (8), 743–746. doi:10.1130/0091-7613(1995)023<0743:WBTUEO>2.3.CO;2

Hacker, B. R., Ratschbacher, L., Webb, L., Ireland, T., Walker, D., and Shuwen, D. (1998). U/Pb zircon ages constrain the architecture of the ultrahigh-pressure Qinling–Dabie Orogen, China. *Earth Planet. Sci. Lett.* 161 (1-4), 215–230. doi:10.1016/S0012-821X(98)00152-6

Hacker, B. R., Ratschbacher, L., Webb, L., McWilliams, M. O., Ireland, T., Calvert, A., et al. (2000). Exhumation of ultrahigh-pressure continental crust in east central China: late Triassic-Early Jurassic tectonic unroofing. *J. Geophys. Res. Solid Earth* 105, 13339–13364. B6. doi:10.1029/2000JB900039

Hanmer, S., Mengel, F., Connelly, J., and Van Gool, J. (1997). Significance of crustal-scale shear zones and synkinematic mafic dykes in the Nagssugtoqidian orogen, SW Greenland: a re-examination. *J. Struct. Geol.* 19 (1), 59–75. doi:10.1016/S0191-8141(96)00078-8

Harrison, T. M., Duncan, I., and McDougall, I. (1985). Diffusion of 40Ar in biotite: temperature, pressure and compositional effects. *Geochimica Cosmochimica Acta* 49 (11), 2461–2468. doi:10.1016/0016-7037(85)90246-7

He, X., Zhang, L., Kagi, H., Smyth, J., Komatsu, K., Li, X., et al. (2022). *In-situ* high-pressure and high-temperature spectroscopic studies of phengite in ultrahigh-pressure eclogite: implications for water transport during ultra-deep continental subduction. *Phys. Chem. Minerals* 49, 24. doi:10.1007/s00269-022-01196-4

He, Y., Li, S., Hoefs, J., Huang, F., Liu, S.-A., and Hou, Z. (2011). Post-collisional granitoids from the Dabie orogen: new evidence for partial melting of a thickened continental crust. *Geochimica Cosmochimica Acta* 75 (13), 3815–3838. doi:10.1016/j.gca.2011.04.011

Hoskin, P. W. O., and Schaltegger, U. (2003). The composition of zircon and igneous and metamorphic petrogenesis. *Rev. Mineralogy Geochem.* 53 (1), 27–62. doi:10.2113/0530027

Hou, Q., Liu, Q., Li, J., and Zhang, H. (2007). Late mesozoic shear zones and its chronology in the dabie mountains, Central China. *Sci. Geol. Sin.* 42, 114–123. (in Chinese with English abstract).

Hou, Q., Zhang, H., Liu, Q., Li, J., and Wu, Y. (2012). The dabie extensional tectonic system: structural framework. *J. Geol. Res.* 2012, 1–8. doi:10.1155/2012/369513

Huang, P., Song, C., Ren, S., Lin, S., Zhang, Y., Li, J., et al. (2016). Tectonic property of the Beihuaiyang tectonic belt and its implications for the location of the suture zone between Yangtze block and North China block. *Acta Geol. Sin.* 90 (6), 1112–1129. (in Chinese with English abstract).

Huang, P., Song, C., Xiao, W., Li, J., Zhou, K., Wang, J., et al. (2021). The geological significance of the deformation and geochronology of the xiaotian–mozitan shear zone in the dabie orogenic belt (east-Central China). *Acta Geol. Sin. - Engl. Ed.* 95 (2), 370–392. doi:10.1111/1755-6724.14652

Ji, W., Lin, W., Faure, M., Shi, Y., and Wang, Q. (2017). The early Cretaceous orogen-scale Dabieshan metamorphic core complex: implications for extensional collapse of the Triassic HP–UHP orogenic belt in east-central China. *Int. J. Earth Sci.* 106, 1311–1340. doi:10.1007/s00531-016-1311-6

Jiang, S., Gao, S., Li, S., Cao, W., Wang, G., Zhang, H., et al. (2017). Gravity-magnetic anomaly and tectonic units in west pacific continent-ocean connection zone. *Earth Sci. Front.* 24, 152–170. doi:10.13745/j.esf.yx.2017-3-24

Jolivet, L., Sautter, V., Moretti, I., Vettor, T., Papadopoulou, Z., Augier, R., et al. (2021). Anatomy and evolution of a migmatite-cored extensional metamorphic dome and interaction with syn-kinematic intrusions, the Mykonos-Delos-Rheneia MCC. *J. Geodyn.* 144, 101824. doi:10.1016/j.jog.2021.101824

Law, R. D. (2014). Deformation thermometry based on quartz c-axis fabrics and recrystallization microstructures: a review. *J. Struct. Geol.* 66, 129–161. doi:10.1016/j.jsg.2014.05.023

Li, S., He, Y., and Wang, S. (2013). Process and mechanism of mountain-root removal of the Dabie Orogen—constraints from geochronology and geochemistry of post-collisional igneous rocks. *Chin. Sci. Bull.* 58 (35), 4411–4417. doi:10.1007/s11434-013-6065-y

Li, S., Huang, F., and Li, H. (2002). Post-collisional lithosphere delamination of the Dabie-Sulu orogen. *Chin. Sci. Bull.* 47 (3), 259–263. doi:10.1360/02tb9063

Li, S., Jagoutz, E., Chen, Y., and Li, Q.-L. (2000). Sm-Nd and Rb-Sr isotopic chronology and cooling history of ultrahigh pressure metamorphic rocks and their country rocks at Shuanghe in the Dabie Mountains, Central China. *Geochimica Cosmochimica Acta* 64, 1077–1093. doi:10.1016/S0016-7037(99)00319-1

Li, S., Kusky, T. M., Wang, L., Zhang, G., Lai, S., Liu, X., et al. (2007). Collision leading to multiple-stage large-scale extrusion in the Qinling orogen: insights from the Mianlue suture. *Gondwana Res.* 12 (1), 121–143. doi:10.1016/j.gr.2006.11.011

Li, S., Suo, Y., Li, X., Zhou, J., Santosh, M., Wang, P., et al. (2019). Mesozoic tectono-magmatic response in the East Asian ocean-continent connection zone to subduction of the Paleo-Pacific Plate. *Earth-Science Rev.* 192, 91–137. doi:10.1016/j.earscirev.2019.03.003

Li, S.-Q., Schmitt, A. K., and Chen, F. (2021). Early Cretaceous mafic–intermediate dykes in the Dabie orogen as indicators for post-collisional lithosphere removal. *Lithos* 388-389, 106065. doi:10.1016/j.lithos.2021.106065

Li, S. Z., Zhao, G. C., Zhang, G. W., Liu, X. C., Dong, S. W., Wang, Y. J., et al. (2010). Not all folds and thrusts in the Yangtze foreland thrust belt are related to the Dabie Orogen: Insights from Mesozoic deformation south of the Yangtze River. *Geol. J.* 45 (5–6), 650–663. doi:10.1002/gj.1214

Li, Z. X., Li, X. H., Kinny, P. D., Wang, J., Zhang, S., and Zhou, H. (2003). Geochronology of Neoproterozoic syn-rift magmatism in the Yangtze Craton, South China and correlations with other continents: evidence for a mantle superplume that broke up Rodinia. *Precambrian Res.* 122 (1), 85–109. doi:10.1016/S0301-9268(02)00208-5

Lin, W., Ji, W., Faure, M., Wu, L., Li, Q., Shi, Y., et al. (2015). Early Cretaceous extensional reworking of the Triassic HP–UHP metamorphic orogen in Eastern China. *Tectonophysics* 662, 256–270. doi:10.1016/j.tecto.2015.05.028

Lin, W., Shi, Y., and Wang, Q. (2009). Exhumation tectonics of the HP-UHP orogenic belt in Eastern China: new structural–petrological insights from the Tongcheng massif, Eastern Dabieshan. *Lithos* 109 (3), 285–303. doi:10.1016/j.lithos.2008.10.007

Lin, W., Wang, Q., Faure, M., and Arnaud, N. (2005). Tectonic evolution of the Dabieshan orogen: in the view from polyphase deformation of the Beihuaiyang metamorphic zone. *Sci. China Ser. D Earth Sci.* 35 (2), 127–139. doi:10.1360/03yd0306

Liou, J., Zhang, R., and Jahn, B.-m. (2000). Petrological and geochemical characteristics of ultrahigh-pressure metamorphic rocks from the dabie-sulu terrane, east-Central China. *Int. Geol. Rev. - Int. Geol. Rev.* 42, 328–352. doi:10.1080/00206810009465086

Liu, F., Gerdes, A., Zeng, L., and Xue, H. (2008). SHRIMP U–Pb dating, trace elements and the Lu–Hf isotope system of coesite-bearing zircon from amphibolite in the SW Sulu UHP terrane, eastern China. *Geochimica Cosmochimica Acta* 72 (12), 2973–3000. doi:10.1016/j.gca.2008.04.007

Liu, F., Xu, Z., Liou, J. G., and Song, B. (2004). SHRIMP U–Pb ages of ultrahigh-pressure and retrograde metamorphism of gneisses, south-western Sulu terrane, eastern China. *J. Metamorph. Geol.* 22 (4), 315–326. doi:10.1111/j.1525-1314.2004.00516.x

Liu, F. L., and Xue, H. M. (2007). Review and prospect of SHRIMP U-Pb dating on zircons from Sulu-Dabie UHP metamorphic rocks. *Acta Petrol. Sin.* 23 (11), 2737–2756. (in Chinese with English abstract).

Liu, X., Jahn, B.-M., and Li, S. (2013). Diachroneity of continental subduction and exhumation: constraints from the Permian-Triassic HP metamorphic terrane in the Tongbai orogen, central China. *Chin. Sci. Bull.* 58 (35), 4397–4404. doi:10.1007/s11434-013-6067-9

Liu, X., and Yan, J. (2020). Geochronology and geochemistry of the sikongshan intrusion in the dabie orogen, Central China: implication for mesozoic geodynamic background. *Geol. J.* 55 (4), 3010–3035. doi:10.1002/gj.3536

Liu, Y., Li, S., Zhai, Q., Tang, Y., Hu, P., Guo, R., et al. (2022). Jurassic tectonic evolution of Tibetan plateau: a review of bangong-nujiang Meso-Tethys Ocean. *Earth-Science Rev.* 227, 103973. doi:10.1016/j.earscirev.2022.103973

Liu, Y. C., Gu, X. F., Rolfo, F., and Chen, Z. Y. (2011). Ultrahigh-pressure metamorphism and multistage exhumation of eclogite of the Luotian dome, North Dabie Complex Zone (central China): evidence from mineral inclusions and decompression textures. *J. Asian Earth Sci.* 42 (4), 607–617. doi:10.1016/j.jseaes.2010.10.016

Liu, Y. C., Li, S. G., and Xu, S. T. (2007). Zircon SHRIMP U–Pb dating for gneisses in northern Dabie high T/P metamorphic zone, central China: implications for decoupling within subducted continental crust. *Lithos* 96 (1), 170–185. doi:10.1016/j.lithos.2006.09.010

Maruyama, S., Liou, J. G., and Zhang, R. (1994). Tectonic evolution of the ultrahigh-pressure (UHP) and high-pressure (HP) metamorphic belts from central China. *Isl. Arc* 3 (2), 112–121. doi:10.1111/j.1440-1738.1994.tb00099.x

Meng, Q.-R., Wei, H.-H., Wu, G.-L., and Duan, L. (2014). Early Mesozoic tectonic settings of the northern North China craton. *Tectonophysics* 611, 155–166. doi:10.1016/j.tecto.2013.11.015

Metcalfe, I. (2013). Gondwana dispersion and Asian accretion: tectonic and palaeogeographic evolution of eastern Tethys. *J. Asian Earth Sci.* 66, 1–33. doi:10.1016/j.jseaes.2012.12.020

Nzenti, J. P., Kapajika, B., Wörner, G., and Lubala, T. R. (2006). Synkinematic emplacement of granitoids in a Pan-African shear zone in Central Cameroon. *J. Afr. Earth Sci.* 45 (1), 74–86. doi:10.1016/j.jafrearsci.2006.01.005

Okay, A., Sengor, A. M. C., and Satir, M. (1993). Tectonics of an ultrahigh-pressure metamorphic terrane: the Dabie Shan/Tongbai Shan Orogen, China. *Tectonics* 12 (6), 1320–1334. doi:10.1029/93TC01544

Oriolo, S., Wemmer, K., Oyhantçabal, P., Fossen, H., Schulz, B., and Siegesmund, S. (2018). Geochronology of shear zones – a review. *Earth-Science Rev.* 185, 665–683. doi:10.1016/j.earscirev.2018.07.007

Passchier, C. W., and Trouw, R. A. J. (2005). *Microtectonics*. Berlin, Heidelberg: Springer, 45–153.

Ratschbacher, L., Franz, L., Enkelmann, E., Jonckheere, R., Pörschke, A., Hacker, B. R., et al. (2006). "The sino-Korean–Yangtze suture, the huwan detachment, and the paleozoic–tertiary exhumation of (ultra)high-pressure rocks along the tongbai-xinxian-dabie mountains," in *Ultrahigh-pressure metamorphism: deep continental subduction* (Colorado, United States: Geological Society of America), 45–75. doi:10.1130/2006.2403(03

Ratschbacher, L., Hacker, B., Webb, L., McWilliams, M., Ireland, T., Dong, S.-J., et al. (2000). Exhumation of the ultrahigh-pressure continental crust in east central China: cretaceous and Cenozoic unroofing and the Tan-Lu fault. *J. Geophys. Res.* 105, 13303–13338. doi:10.1029/2000JB900040

Rey, P. F., Teyssier, C., and Whitney, D. L. (2009). The role of partial melting and extensional strain rates in the development of metamorphic core complexes. *Tectonophysics* 477 (3), 135–144. doi:10.1016/j.tecto.2009.03.010

Ring, U., and Collins, A. S. (2005). U–Pb SIMS dating of synkinematic granites: timing of core-complex formation in the northern Anatolide belt of western Turkey. *J. Geol. Soc.* 162 (2), 289–298. doi:10.1144/0016-764904-016

Rubatto, D. (2017). Zircon: the metamorphic mineral. *Rev. Mineralogy Geochem.* 83 (1), 261–295. doi:10.2138/rmg.2017.83.9

Schmid, J. C., Ratschbacher, L., Hacker, B. R., Gaitzsch, I., and Dong, S. (1999). How did the foreland react? Yangtze foreland fold-and-thrust belt deformation related to exhumation of the Dabie Shan ultrahigh-pressure continental crust (eastern China). *Terra nova.* 11 (6), 266–272. doi:10.1046/j.1365-3121.1999.00254.x

Shi, Y., Lin, W., Ji, W., and Wang, Q. (2014). The architecture of the HP–UHP Dabie massif: new insights from geothermobarometry of eclogites, and implication for the continental exhumation processes. *J. Asian Earth Sci.* 86, 38–58. doi:10.1016/j.jseaes.2013.09.005

Sorokin, A. A., Zaika, V. A., Kovach, V. P., Kotov, A. B., Xu, W., and Yang, H. (2020). Timing of closure of the eastern Mongol–Okhotsk Ocean: constraints from U–Pb and Hf isotopic data of detrital zircons from metasediments along the Dzhagdy Transect. *Gondwana Res.* 81, 58–78. doi:10.1016/j.gr.2019.11.009

Suo, S. T., Zhong, Z. Q., and You, Z. D. (2001). Extensional tectonic framework of the Dabie - sulu UHP-HP metamorphic belt, Central China, and its geodynamical significance. *Acta Geol. Sin.* 75 (1), 14–24. (in Chinese with English abstract).

Vanderhaeghe, O. (2001). Melt segragation, pervasive melt migration and magma mobility in the continental crust: the structural record from pores to orogens. *Phys. Chem. Earth, Part A Solid Earth Geodesy* 26 (4), 213–223. doi:10.1016/S1464-1895(01)00048-5

Walte, N. P., Bons, P. D., and Passchier, C. W. (2005). Deformation of melt-bearing systems—insight from *in situ* grain-scale analogue experiments. *J. Struct. Geol.* 27 (9), 1666–1679. doi:10.1016/j.jsg.2005.05.006

Wan, Y., Li, R., Wilde, S. A., Liu, D., Chen, Z., Yan, L., et al. (2005). UHP metamorphism and exhumation of the Dabie Orogen, China: evidence from SHRIMP dating of zircon and monazite from a UHP granitic gneiss cobble from the Hefei Basin. *Geochimica Cosmochimica Acta* 69 (17), 4333–4348. doi:10.1016/j.gca.2005.03.055

Wang, F. N., Genser, J., and Yang, W. R. (1998). The Dabie UHP unit, Central China: a Cretaceous extensional allochthon superposed on a Triassic orogen. *Terra nova.* 10 (5), 260–267. doi:10.1046/j.1365-3121.1998.00200.x

Wang, Q., Wyman, D. A., Xu, J., Jian, P., Zhao, Z., Li, C., et al. (2007). Early Cretaceous adakitic granites in the Northern Dabie Complex, central China: implications for partial melting and delamination of thickened lower crust. *Geochimica Cosmochimica Acta* 71 (10), 2609–2636. doi:10.1016/j.gca.2007.03.008

Wang, T., Zheng, Y., Zhang, J., Zeng, L., Donskaya, T., Guo, L., et al. (2011). Pattern and kinematic polarity of late Mesozoic extension in continental NE Asia: perspectives from metamorphic core complexes. *Tectonics* 30 (6), 1–27. doi:10.1029/2011TC002896

Wang, X., Liou, J., and Mao, H.-k. (1989). Coesite-bearing eclogite from the dabie mountains in central China. *Geology* 17 (12), 1085–1088. doi:10.1130/0091-7613(1989)017<1085:CBEFTD>2.3.CO;2

Wang, X. M., Zhang, R., and Liou, J. (1995). *UHPM terrane in east central China, Ultrahigh pressure metamorphism*. Cambridge: Cambridge University Press, 356–390. doi:10.1017/CBO9780511573088.011

Wang, Y., Bai, Q., and Yang, B. (2018). Structural characteristics and geochronology of migmatites in the North Dabie Complex unit: timing of post-collisional deformation. *Sci. China Earth Sci.* 61 (7), 887–902. doi:10.1007/s11430-017-9189-6

Wang, Y., Sheng, Y., Xiang, B., and Zhang, C. (2012). Metamorphic pressure of the luzhenguan Group in the North huaiyang low-grade metamorphic belt and its indication for evolution of the dabie mountains. *Geol. Rev.* 58 (5), 865–872. (Chinese with English abstract).

Wang, Y., Wang, H., Sheng, Y., and Xiang, B. (2014). Early Cretaceous uplift history of the Dabie orogenic belt: evidence from pluton emplacement depths. *Sci. China Earth Sci.* 57 (5), 1129–1140. doi:10.1007/s11430-013-4659-5

Wang, Y., Xiang, B., Zhu, G., and Jiang, D. (2011). Structural and geochronological evidence for Early Cretaceous orogen-parallel extension of the ductile lithosphere in the northern Dabie orogenic belt, East China. *J. Struct. Geol.* 33 (3), 362–380. doi:10.1016/j.jsg.2010.09.002

Wiest, J. D., Osmundsen, P.-T., Jacobs, J., and Fossen, H. (2019). Deep crustal flow within postorogenic metamorphic core complexes: insights from the southern western gneiss region of Norway. *Tectonics* 38, 4267–4289. doi:10.1029/2019TC005708

Wu, Y., Tang, J., Zhang, S.-B., and Zhao, Z.-F. (2007c). SHRIMP zircon U-Pb dating for two episodes of migmatization in the Dabie orogen. *Chin. Sci. Bull.* 52 (13), 1836–1842. doi:10.1007/s11434-007-0249-2

Wu, Y. B., Zhang, S. B., Zhao, Z. F., Wu, F. Y., and Liu, X. M. (2007b). Zircon U–Pb ages and Hf isotope compositions of migmatite from the North Dabie terrane in China: constraints on partial melting. *J. Metamorph. Geol.* 25 (9), 991–1009. doi:10.1111/j.1525-1314.2007.00738.x

Wu, Y. B., Zheng, Y. F., Zhang, S. B., Zhao, Z. F., Wu, F. Y., and Liu, X. M. (2007a). Zircon U–Pb ages and Hf isotope compositions of migmatite from the North Dabie terrane in China: constraints on partial melting. *J. Metamorph. Geol.* 25 (9), 991–1009. doi:10.1111/j.1525-1314.2007.00738.x

Xia, Q. K., Zheng, Y.-F., Ge, N. J., and Deloule, E. (2003). U-Pb ages and oxygen isotope compositions of zircons from gneiss of Huangtuling, Northern Dabie: old protolith and multi-stage evolution. *Acta Petrol. Sin.* 19, 506–512. (in Chinese with English abstract).

Xie, Z., Chen, J. F., and Cui, Y. R. (2010). Episodic growth of zircon in UHP orthogneisses from the North Dabie Terrane of east-central China: implications for crustal architecture of a collisional orogen. *J. Metamorph. Geol.* 28 (9), 979–995. doi:10.1111/j.1525-1314.2010.00902.x

Xu, C., Zhou, Z., Ma, C., and Reiners, P. W. (2002). Geochronological constraints on 140–85 Ma thermal doming extension in the Dabie orogen, central China. *Sci. China Ser. D Earth Sci.* 45 (9), 801–817. doi:10.1007/BF02879515

Xu, H., Ma, C., Song, Y., Zhang, J., and Ye, K. (2012). Early Cretaceous intermediate-mafic dykes in the Dabie orogen, eastern China: petrogenesis and implications for crust–mantle interaction. *Lithos* 154, 83–99. doi:10.1016/j.lithos.2012.06.030

Xu, H., Ma, C., and Ye, K. (2007). Early cretaceous granitoids and their implications for the collapse of the Dabie orogen, eastern China: SHRIMP zircon U–Pb dating and geochemistry. *Chem. Geol.* 240 (3), 238–259. doi:10.1016/j.chemgeo.2007.02.018

Xu, S., Su, W., Liu, Y., Jiang, L., Ji, S., Okay, A. I., et al. (1992). Diamond from the dabie Shan metamorphic rocks and its implication for tectonic setting. *Science* 256 (5053), 80–82. doi:10.1126/science.256.5053.80

Xue, F., Rowley, D. B., Tucker, R. D., and Peng, Z. X. (1997). U-Pb zircon ages of granitoid rocks in the North dabie complex, eastern dabie Shan, China. *J. Geol.* 105 (6), 744–753. doi:10.1086/515984

Xue, H. M., Dong, S., and Liu, X. (2002). U/Pb zircon dating of granitic gneisses in eastern Dabie Mountains, Central China. *Sci. Geol. Sin.* 37, 165–173. (in Chinese with English abstract).

Yang, J. S., Wooden, J. L., Wu, C. L., Liu, F. L., Xu, Z. Q., Shi, R. D., et al. (2003). SHRIMP U–Pb dating of coesite-bearing zircon from the ultrahigh-pressure metamorphic rocks, Sulu terrane, east China. *J. Metamorph. Geol.* 21 (6), 551–560. doi:10.1046/j.1525-1314.2003.00463.x

Yang, Y., Liu, Y.-C., Li, Y., Groppo, C., and Rolfo, F. (2020). Zircon U-Pb dating and petrogenesis of multiple episodes of anatexis in the North dabie complex zone, Central China. *Minerals* 10 (7), 618. doi:10.3390/min10070618

Ye, K., Cong, B., and Ye, D. (2000). The possible subduction of continental material to depths greater than 200 km. *Nature* 407 (6805), 734–736. doi:10.1038/35037566

Yin, A. (2004). Gneiss domes and gneiss dome systems. *Geol. Soc. Am.* 380, 1–24. doi:10.1130/0-8137-2380-9.1

Zhang, C., Holtz, F., Koepke, J., Berndt, J., and Ma, C. (2014). Decompressional anatexis in the migmatite core complex of northern Dabie orogen, eastern China: petrological evidence and Ti-in-quartz thermobarometry. *Lithos* 202-203, 227–236. doi:10.1016/j.lithos.2014.05.024

Zhang, C., Ma, C., Holtz, F., Koepke, J., Wolff, P. E., and Berndt, J. (2013a). Mineralogical and geochemical constraints on contribution of magma mixing and fractional crystallization to high-Mg adakite-like diorites in eastern Dabie orogen, East China. *Lithos* 172-173, 118–138. doi:10.1016/j.lithos.2013.04.011

Zhang, G., Guo, A., Wang, Y., Sanzhong, L., Dong, Y., Liu, S., et al. (2013b). Tectonics of south China continent and its implications. *Sci. China Earth Sci.* 56, 1804–1828. doi:10.1007/s11430-013-4679-1

Zhang, G., Meng, Q., and Yu, Z. (1996). Orogenesis and dynamics of the qinling orogen. *Sci. China (Series D)* 39 (3), 225–234.

Zhang, J., Chen, Z., Yakymchuk, C., Sa, R., Huang, Q., Lou, F., et al. (2023). Early paleozoic crustal anatexis during wuyi-yunkai orogenesis: insights from zircon of fuhuling migmatites in the yunkai region, south China. *Geosphere* 19 (5), 1399–1420. doi:10.1130/GES02638.1

Zhang, J., Ma, C., Li, J., and Pan, Y. (2015). Petrogenesis of Early Cretaceous alkaline dolerite dykes in the Dabie Orogen, China: constraints on the timing of lithospheric thinning. *Lithos* 216-217, 17–30. doi:10.1016/j.lithos.2014.12.002

Zhao, L., Tang, H., Mitchell, R. N., Li, Q. L., Zhou, X. W., and Zhai, M. G. (2023). The joining of north and south China during the permian: coherent metamorphic evidence from east Asia orogenesis. *Coherent Metamorph. Evid. East Asia Orogenesis* 42 (8), e2023TC007916. doi:10.1029/2023TC007916

Zhao, Z. F., Zheng, Y. F., and Wei, C. S. (2004). Zircon U-Pb age, element and oxygen isotope geochemistry of mesozoic intermediate-felsic rocks in the dabie mountains. *Acta Petrol. Sin.* 20 (5), 1151–1174. (in Chinese with English abstract).

Zhao, Z.-F., Zheng, Y.-F., Wei, C.-S., Chen, F.-K., Liu, X., and Wu, F.-Y. (2008). Zircon U–Pb ages, Hf and O isotopes constrain the crustal architecture of the ultrahigh-pressure Dabie orogen in China. *Chem. Geol.* 253 (3), 222–242. doi:10.1016/j.chemgeo.2008.05.011

Zhao, Z.-F., Zheng, Y.-F., Wei, C.-S., and Wu, Y.-B. (2007). Post-collisional granitoids from the Dabie orogen in China: zircon U–Pb age, element and O isotope evidence for recycling of subducted continental crust. *Lithos* 93 (3), 248–272. doi:10.1016/j.lithos.2006.03.067

Zhao, Z.-F., Zheng, Y.-F., Wei, C.-S., Wu, Y.-B., Chen, F., and Jahn, B.-m. (2005). Zircon U–Pb age, element and C–O isotope geochemistry of post-collisional mafic-ultramafic rocks from the Dabie orogen in east-central China. *Lithos* 83 (1), 1–28. doi:10.1016/j.lithos.2004.12.014

Zheng, Y. (2004). Position of south China in configuration of neoproterozoic supercontinent. *Chin. Sci. Bull.* 49 (8), 751–753. doi:10.1007/BF02889741

Zheng, Y. (2008). A perspective view on ultrahigh-pressure metamorphism and continental collision in the Dabie-Sulu orogenic belt. *Chin. Sci. Bull.* 53 (20), 3081–3104. doi:10.1007/s11434-008-0388-0

Zheng, Y.-F., Gao, T.-S., Wu, Y.-B., Gong, B., and Liu, X. M. (2007). Fluid flow during exhumation of deeply subducted continental crust: zircon U-Pb age and O-isotope studies of a quartz vein within ultrahigh-pressure eclogite. *Stud. a quartz vein within ultrahigh-pressure eclogite* 25 (2), 267–283. doi:10.1111/j.1525-1314.2007.00696.x

Zheng, Y.-F., Zhao, Z.-F., and Chen, Y.-X. (2013). Continental subduction channel processes: plate interface interaction during continental collision. *Chin. Sci. Bull.* 58, 4371–4377. doi:10.1007/s11434-013-6066-x

Zheng, Y.-F., Zhou, J.-B., Wu, Y.-B., and Xie, Z. (2005). Low-grade metamorphic rocks in the dabie-sulu orogenic belt: a passive-margin accretionary wedge deformed during continent subduction. *Int. Geol. Rev.* 47 (8), 851–871. doi:10.2747/0020-6814.47.8.851

Zhong, Z. Q., Suo, S. T., and You, Z. D. (1998). Extensional tectonic framework of post high and ultrahigh pressure metamorphism in Dabieshan, China. *Earth Sci. - J. China Univ. Geosciences* 23 (3), 225–229. (in Chinese with English abstract).

Zhou, Y.-Z., Han, B.-F., Zhang, B., Xu, Z., Ren, R., Li, X.-W., et al. (2012). The Yingba shear zone on the sino-Mongolian border: southwestern extension of the zuunbayan fault from Mongolia to China and implications for late mesozoic intracontinental extension in eastern Asia. *Tectonophysics* 574-575, 118–132. doi:10.1016/j.tecto.2012.08.042

Zhu, G., Wang, Y., Wang, W., Zhang, S., Liu, C., Gu, C., et al. (2017a). An accreted micro-continent in the north of the Dabie Orogen, East China: evidence from detrital zircon dating. *Tectonophysics* 698, 47–64. doi:10.1016/j.tecto.2017.01.004

Zhu, R., and Xu, Y. (2019). The subduction of the west Pacific plate and the destruction of the North China Craton. *Sci. China Earth Sci.* 62 (9), 1340–1350. doi:10.1007/s11430-018-9356-y

Zhu, R., Zhang, H., Zhu, G., Meng, Q., Fan, H., Yang, J., et al. (2017b). Craton destruction and related resources. *Int. J. Earth Sci.* 106 (7), 2233–2257. doi:10.1007/s00531-016-1441-x